Identification of backed flakes in Discoid and RCLevallois

Combining quantitative approaches to differentiate between backed products from discoidal and Levallois reduction sequences

Guillermo Bustos-Pérez[1]
Brad Gravina[2,3]
Michel Brenet[3,4]
Francesca Romagnoli[1]

[1]Universidad Autónoma de Madrid. Departamento de Prehistoria y Arqueología, Campus de Cantoblanco, 28049 Madrid, Spain
[2]Musée national de Préhistoire, MCC, 1 rue du Musée, 24260 Les Eyzies de Tayac, France
[3]UMR-5199 PACEA, Université de Bordeaux, Bâtiment B8, Allée Geoffroy Saint Hilaire, CS 50023, 33615 PESSAC CEDEX, France
[4]INRAP Grand Sud-Ouest, Centre mixte de recherches archéologiques, Domaine de Campagne, 242460 Campagne, France

Corresponding authors:
G.B.P. guillermo.willbustos@mail.com
F.R. f.romagnoli2@gmail.com

Abstract

Backed flakes (core edge flakes and pseudo-Levallois points) represent special products of Middle Paleolithic centripetal flaking strategies. Their peculiarities are due to their roles as both a technological objective and in the management of core convexities to retain its geometric properties during reduction. In Middle Paleolithic contexts, these backed implements are commonly produced within Levallois and discoidal reduction sequences. Often, Levallois and discoidal backed implements show common geometric and morphological features that complicate their attribution to one of these methods. This study examines the identification of experimentally produced discoidal and recurrent centripetal Levallois backed products (including all stages of reduction) based on their morphological features. 3D geometric morphometrics are employed to quantify morphological variability among the experimental sample. Dimensionality reduction though principal component analysis is combined with 11 machine learning models for the identification of knapping methods. A supported vector machine with polynomial kernel has been identified as the best model (with a general accuracy of 0.76 and an area under the curve [AUC] of 0.8). This indicates that combining geometric morphometrics, principal component analysis, and machine learning models succeeds in capturing the morphological differences of backed products according to the knapping method.

Key words: lithic analysis; Levallois; Discoid; Geometric Morphometrics; Machine Learning; Deep Learning

1. Introduction

The Middle Paleolithic in Western Europe is characterized by the diversification and increase of knapping methods resulting in flake-dominated assemblages (Delagnes and Meignen, 2006; Kuhn, 2013). Two of the most common flake production methods are the Discoid and the Levallois recurrent centripetal.
Following Boëda (1995a, 1994, 1993), there are six technological defining criteria defining the Discoid method:

1. The volume of the core is conceived as two oblique asymmetric convex surfaces delimited by an intersection plane;

2. These two surfaces are not hierarchical being possible to alternate the roles of percussion and exploitation surfaces;

3. The peripheral convexity of the debitage surface is managed to control lateral and distal extractions thus allowing for a degree of predetermination;

4. Surfaces of the striking planes are oriented in a way that the core edge is perpendicular to the predetermined products;

5. The planes of extraction of the products are secant;

6. The technique employed is the direct percussion with hard hammer.

Also, according to Boëda (1994, 1993) six characteristics define the Levallois knapping strategy from a technological point of view:

1. The volume of the core is conceived in two convex asymmetric surfaces;

2. These two surfaces are hierarchical and are not interchangeable. They maintain their role of striking and debitage (or exploitation) surface respectively along the whole reduction process;

3. The distal and lateral convexities of the debitage surface are maintained to obtain predetermined flakes;

4. The plane of fracture of the predetermined products is parallel to the intersection between both surfaces;

5. The striking platform is perpendicular to the overhang (the core edge, at the intersection between the two core surfaces);

6. The technique employed during the knapping process is the direct percussion with hard hammer.

Depending on the organization of the debitage surface Levallois cores are usually classified into preferential method (were a single predetermined Levallois flake is obtained from the debitage surface) or recurrent methods (were several predetermined flakes are produced from the debitage surface) with removals being either unidirectional, bidirectional or centripetal (Boëda, 1995a; Delagnes, 1995; Delagnes and Meignen, 2006). Both knapping methods share the production of backed products which usually includes two wide categories: core edge flakes (*eclat débordant*) and pseudo-Levallois points.
Core edge flakes / *eclat débordant* (Beyries and Boëda, 1983; Boëda, 1993; Boëda et al., 1990) are technical backed knives which have a cutting edge opposite and parallel to a blunt margin (which usually haves an angle close to the 90º). This blunt margin commonly results from the removal of one of the laterals of the core and can be plain, keep the scars from previous removals or be cortical. Core edge flakes are also divided into two categories: "classical core edge flakes" and "core edge flakes with a limited back." "Classical core edge flakes" (Beyries and Boëda, 1983; Boëda, 1993; Boëda et al., 1990), which are sometimes referred to as "core edge flakes with a non-limited back"/*"éclat débordant à dos non limité"* (Duran, 2005; Duran and Soler, 2006), have a morphological axis more or less similar to the axis of percussion. "Core edge flakes with a limited back"/*"éclat débordant à dos limité"* have a deviated axis of symmetry regarding the axis of percussion (Meignen, 1996; Meignen, 1993; Pasty et al., 2004). Usually, because of this deviation, the back is not parallel and does not span the entire length of the sharp edge or the percussion axis (Slimak, 2003).
Pseudo-Levallois points (Boëda, 1993; Boëda et al., 1990; Bordes, 1961, 1953; Slimak, 2003) are backed products where the edge opposite to the back has a triangular morphology. This triangular morphology is usually the result of the convergence of two or more scars. As with core edge flakes, the back usually

results from the removal of one of the lateral edges of the core and can be plain, retain the scars from previous removals, or more rarely be cortical. Both pseudo-Levallois points and core edge flakes with a limited back share the deviation of symmetry from the axis of percussion but are clearly differentiable due to their morphology. The present study includes the three categories defined above as backed products.
Depending on the knapping method, different roles in Levallois recurrent centripetal and discoidal debitage are attributed to core edge flakes and pseudo-Levallois points. Boëda et al. (1990) focus on the role of core edge flakes and cortically backed flakes for maintaining the lateral convexities throughout Levallois recurrent centripetal reduction. Similarly, pseudo-Levallois points contribute to maintaining the lateral and distal convexities between different series of removals (Boëda et al., 1990).
Focusing on the variability of discoidal, debitage Slimak (2003) points out that pseudo-Levallois points are short products that induce a limited lowering of the core overhang (the intersection between the striking and debitage surfaces). In contrast, core edge flakes can result from several distinct production objectives. Expanding on the roles of pseudo-Levallois points and core edge flakes within discoidal debitage, Locht (2003) demonstrated the systematic production of both products at the site of Beauvais. This indicates that at Beauvais, core edge flakes and pseudo-Levallois points were the main predetermining/predetermined products (Locht, 2003).
An additional added value of core edge flakes and pseudo-Levallois points is their frequent transport by Paleolithic groups. Turq et al. (2013) described the widespread import and export of lithic artifacts during the Middle Paleolithic. Examples of the transport of pseudo-Levallois points from discoidal production sequences can be observed at Combemenue, La Mouline, Les Fieux (Brenet, 2013, 2012; Brenet and Cretin, 2008; Folgado and Brenet, 2010; Turq et al., 2013), and the open-air site of Bout des Vergnes (Courbin et al., 2020), while the transport of core edge flakes (into and out of the site) is also clearly observed at la Grotte Vaufrey (Geneste, 1988) and at Site N of Maastricht-Belvédère (Roebroeks et al., 1992). Transported backed pieces have also been clearly identified at Abric Romaní in Spain within both Levallois and discoidal production methods (Martín-Viveros et al., 2020; Romagnoli et al., 2016).

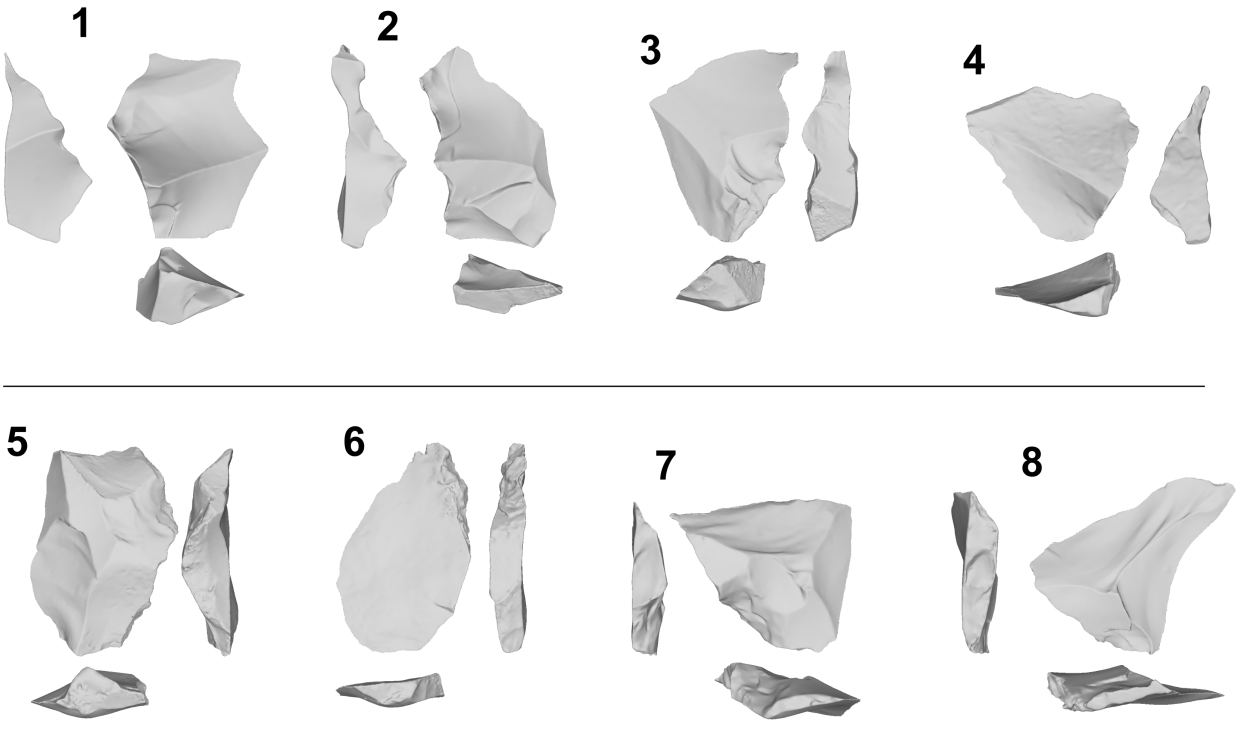

Figure 1: Backed products from the experimental sample: core edge flakes (1–2) and pseudo-Levallois points (3–4) from the Discoid knapping method. Core edge flakes (5–6) and pseudo-Levallois points (7–8) from the Levallois recurrent centripetal method

A problem exists in the attribution of backed pieces to either discoidal or recurrent centripetal Levallois reduction. Mourre (2003) indicates that a key aspect for the identification of Levallois core edge flakes is the direction of the debitage axis, which is parallel to the intersection plane of the two core surfaces while the fracture plane is secant. Slimak (1998) indicates that core edge flakes from the discoidal method might have fracture planes parallel to the intersection between the debitage and striking surfaces although not as parallel as in Levallois debitage. Delpiano et al. (2021) indicate that Levallois artifacts tend to be more elongated with thinner and sub-parallel edges, whereas discoidal backed products show higher variation in the minimum and maximum thickness of the back.
This raises the question as to the extent to which Discoid and Levallois recurrent centripetal core edge flakes and pseudo-Levallois points can be differentiated based on their morphological features. This issue is relevant in lithic studies because it affects the technological analysis of a stone tool assemblage and the evolutionary interpretation of knapping concepts over time. In this paper, we address this issue through experimental archaeology and a multi-level statistical approach. We reproduced classic bifacial discoidal and recurrent centripetal Levallois reduction sequences to obtain a collection of backed products. 3D scanning of lithic artifacts and geometric morphometrics was employed to quantify the morphological variability of the experimental sample and the cores were refit. On the set of coordinates, dimensionality reduction through principal component analysis (PCA) was carried out, and 11 machine learning models were tested to obtain classification accuracy and variable importance.

2 Methods

2.1 Experimental assemblage

The analyzed experimental assemblage derives from the replication of nine discrete knapping sequences. Seven cores were knapped in Bergerac chert (Fernandes et al., 2012), and two cores were knapped in Miocene chert from South of Madrid (Bustillo et al., 2012; Bustillo and Pérez-Jiménez, 2005). Five cores were knapped following the discoidal *"sensu stricto"* method, which corresponds highly to Boëda's original technological definition of the knapping system (Boëda, 1995b, 1994, 1993), and five experimental cores were knapped following the Levallois recurrent centripetal system (Boëda, 1995a, 1994, 1993; Lenoir and Turq, 1995). A total of 139 unretouched backed flakes (independent of the type of termination) were obtained: 70 from the discoidal reduction sequences and 69 from the Levallois reduction sequences (Figure 1). In the case of the Levallois recurrent centripetal cores, backed products from both debitage and striking surfaces were included.

The following code loads data and packages necessary for the development of the present research.

```
# List of packages
list.of.packages <- c("tidyverse", "caret",  "ranger")

# Load packages
lapply(list.of.packages, library, character.only = TRUE)
```

```
## [[1]]
##  [1] "forcats"   "stringr"   "dplyr"     "purrr"     "readr"     "tidyr"
##  [7] "tibble"    "ggplot2"   "tidyverse" "stats"     "graphics"  "grDevices"
## [13] "utils"     "datasets"  "methods"   "base"
##
## [[2]]
##  [1] "caret"     "lattice"   "forcats"   "stringr"   "dplyr"     "purrr"
##  [7] "readr"     "tidyr"     "tibble"    "ggplot2"   "tidyverse" "stats"
## [13] "graphics"  "grDevices" "utils"     "datasets"  "methods"   "base"
##
## [[3]]
```

```
##  [1] "ranger"    "caret"     "lattice"   "forcats"   "stringr"   "dplyr"
##  [7] "purrr"     "readr"     "tidyr"     "tibble"    "ggplot2"   "tidyverse"
## [13] "stats"     "graphics"  "grDevices" "utils"     "datasets"  "methods"
## [19] "base"
```

```
rm(list.of.packages)
```

```
# Loading landmarks coordinates
load("Data/Flakes LM rotated.RData")

# Loading manual attributes
Att <- read.csv("Data/Attributes data.csv")
```

The Levallois recurrent centripetal experimental assemblage is clearly dominated by non-cortical backed flakes (n = 42; 60.87%). This is expected since one of the roles of core edge flakes and pseudo-Levallois points in Levallois recurrent centripetal methods is the management of convexities on subsequent exploitation sequences (Boëda, 1994, 1993; Boëda et al., 1990). Thus, although backed flakes can be present in the initial decortication phases (n = 9; 13.04%), the subsequent exploitation of the core will result in non-cortical flakes. Non-cortical backed flakes are also the majority class of the experimental Discoid assemblage although this predominance is attenuated (n = 29; 41.43%). However, along with flakes with nearly 25% of the dorsal surface covered with cortex, they make up the majority of the discoidal backed flakes of the assemblage (n = 51; 72.86%). This reduction in the predominance of non-cortical flakes is also expected in discoidal methods given the organization of both debitage surfaces, the nature of the surface convexities, and the fracture plane. In discoidal cores, both interchangeable surfaces usually have a higher apical convexity than Levallois cores. Additionally, the angle and removal of flakes cover a smaller portion of the respective surface than in a Levallois core. Thus, it is expected that further into the knapping sequence, some products will retain a certain amount of cortex.

```
# Cortex per method in backed flakes
Att %>% group_by(Strategy) %>%
  count(CORTEX) %>%
  mutate(Percentage = round(n/sum(n)*100, 2)) %>%
  ggplot(aes(CORTEX, Percentage, fill = Strategy)) +
  geom_col(position = "dodge") +
  ggsci::scale_fill_aaas() +
  xlab(NULL) +
  geom_text(aes(label = paste0(Percentage, "%")),
            vjust= -0.2, size = 2.5,
            position = position_dodge(.9)) +
  geom_text(aes(label = paste("n =", n)),
            vjust = "top", size = 2.5,
            position = position_dodge(.9)) +
  theme_classic() +
  theme(
    legend.position = "bottom",
    axis.text = element_text(color = "black", size = 8))
```

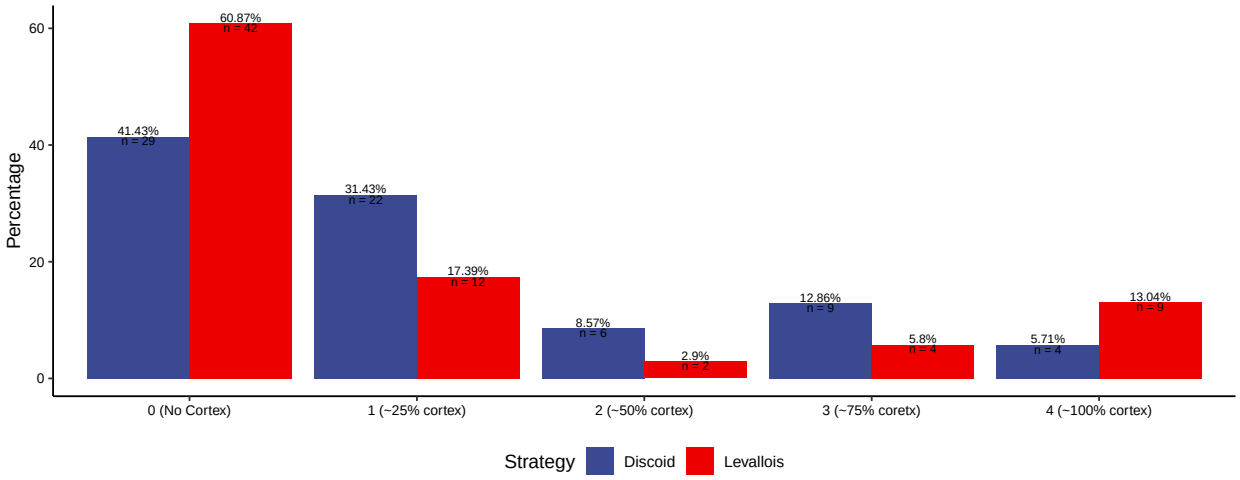

2.2 Data acquisition

All flakes were scanned with an Academia 20 structured light surface scanner (Creaform 3D) at a 0.2 mm resolution. Flakes were scanned in two parts and automatically aligned (or manually aligned in case automatic alignment failed) and exported in STL formats. Cloudcompare 2.11.3 (https://www.danielgm.net/cc/) free software was employed to perform additional cleaning, mesh sampling, surface reconstruction, and transformation into PLY files. Finally, all files were decimated to a quality of 50,000 faces using the Rvcg R package (Schlager, 2017).

The protocol for the digitalization of landmarks on flakes was based on previous studies (Archer et al., 2021, 2018). This included the positioning of a total of 3 fixed landmarks, 85 curve semi-landmarks, and 420 surface semi-landmarks (Bookstein, 1997a, 1997b; Gunz et al., 2005; Gunz and Mitteroecker, 2013; Mitteroecker and Gunz, 2009). This makes for a total of 508 landmarks and semi-landmarks. The three fixed landmarks correspond to both laterals of the platform width, and the percussion point. The 85 curve semi-landmarks correspond to the internal and exterior curve outlines of the platform (15 semi-landmarks each) and the edge of the flake (55 semi-landmarks), and the 60 surface semi-landmarks correspond to the platform surface. The dorsal and ventral surfaces are defined by 180 semi-landmarks each. The workflow for digitalizing the landmarks and semi-landmarks included the creation of a template/atlas on an arbitrary selected flake. After this, the landmarks and semi-landmarks were positioned in each specimen and were relaxed to minimize bending energy (Bookstein, 1997a, 1997b). The entire workflow of landmark and semi-landmarks digitalization and relaxation to minimize bending energy was done in Viewbox version 4.1.0.12 (http://www.dhal.com/viewbox.htm), and resulting point coordinates were exported into .xlsx files.

Procrustes superimposition (Kendall, 1984; Mitteroecker and Gunz, 2009; O'Higgins, 2000) was performed using the package "Morpho" (Schlager, 2017) on RStudio IDE (R. C. Team, 2019; Rs. Team, 2019). After performing Procrustes superimposition and obtaining a new set of coordinates, PCA was performed to reduce the dimensionality of the data (James et al., 2013; Pearson, 1901). There are multiple reasons to use dimensionality reduction when dealing with high dimensional data on classification, including to avoid having more predictors than observations ($p > n$), to avoid the collinearity of predictors, to reduce the dimensions of the feature space, and to avoid overfitting due to an excessive number of degrees of freedom (simple structure with lower number of variables). PCA achieves dimensionality reduction by identifying the linear combinations that best represent the predictors in an unsupervised manner. The principal components (PCs) of a PCA are aimed to capture as high a variance as possible of the complete data (James et al., 2013), and PCs that capture a higher variance do not necessarily need to be the best for classification. For the present work, PCs that represent 95% of the variance were selected as predictors for training the machine learning models. The threshold of 95% of the variance was arbitrarily selected since it balances retaining most of the dataset variance on a reduced number of variables. The identification of best PCs for classification was automatically done by the machine learning models using the caret package (Kuhn, 2008).

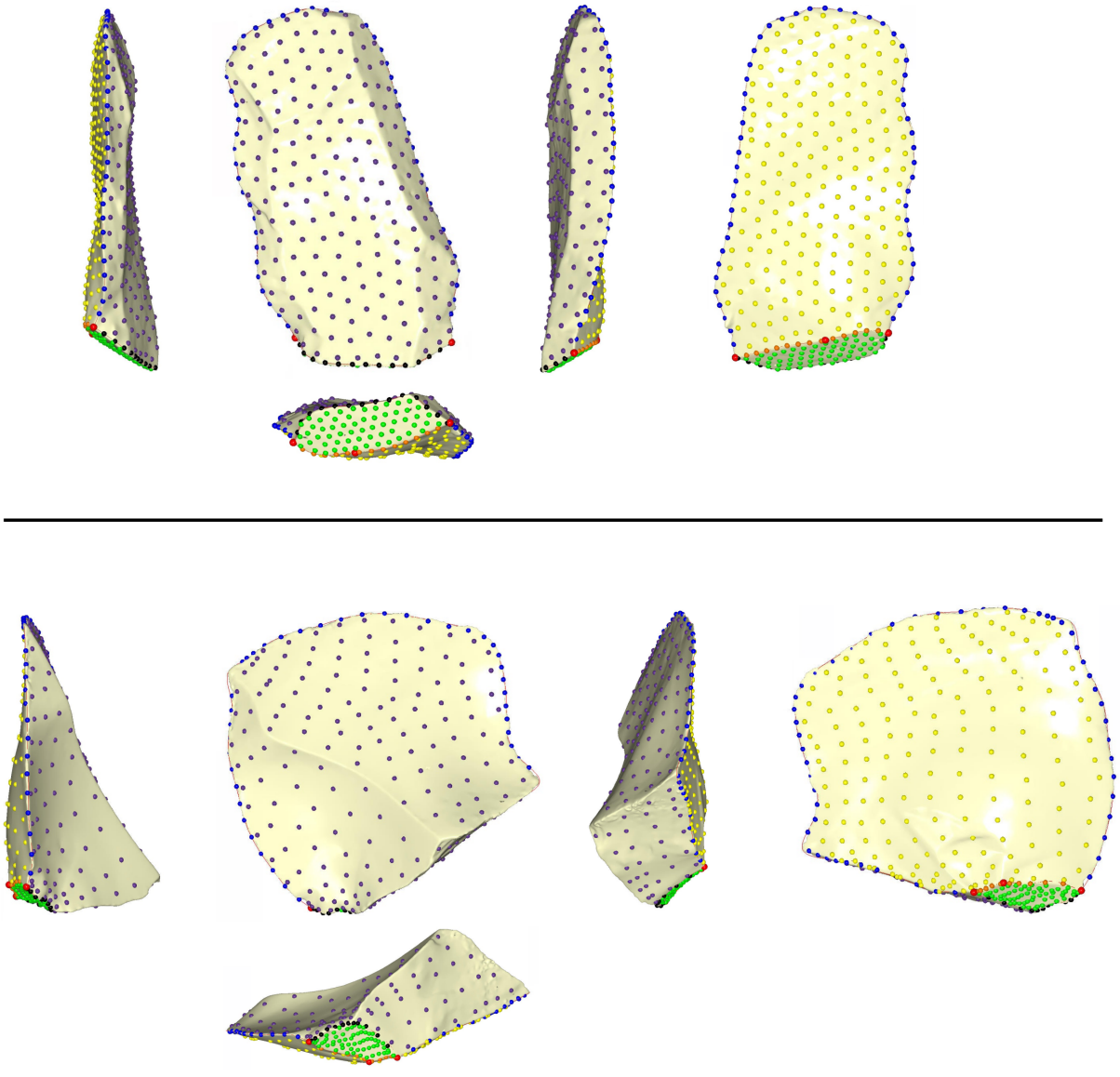

Figure 2: Template/atlas on an arbitrary selected flake with the defined landmarks (in red), curves, and surfaces. Bottom: Landmark positioning after sliding to minimize bending energy on a pseudo-Levallois point from a discoidal reduction sequence.

In addition to geometric morphometrics, the following attributes were recorded for each of the flakes using the E5 software (McPherron, 2019).

- **Technological length:** measured in mm along the axis perpendicular to the striking platform.
- **Technological width:** measured in mm along the axis perpendicular to the technological width.
- **Maximum thickness** of the flake measured in mm.
- **External platform angle (EPA):** measured in degrees with a manual goniometer.
- **Internal platform angle (EPA):** measured in degrees with a manual goniometer.
- **Relative amount of cortex on the dorsal face**: recorded according to its extension on the dorsal surface of the flake, with categories as follows: 0 (no cortex), 1 (nearly 25% covered by cortex), 2 (nearly 50% covered by cortex), 3 (nearly 75% covered by cortex), and 4 (nearly the entire surface covered by cortex). This variable was employed to evaluate the distribution of cortex proportions among the experimental assemblage.
- **Weight**: measured to a precision of 0.01 g.

These measures served to generate the following indices:

- **Elongation index**: length divided by width.
- **Carenation index**: result of dividing either width or length (the one with the lowest value) between maximum thickness.
- **Width to thickness ratio**: flake width divided by maximum thickness.

2.3 Machine learning models and evaluation

The following 11 machine learning models have been tested for differentiating between backed flakes extracted from the two surfaces of the core within each knapping method:

- **Linear discriminant analysis (LDA):** reduces dimensionality aiming to maximize the separation between classes while decision boundaries divide the predictor range into regions (Fisher, 1936; James et al., 2013).
- **K-nearest neighbor (KNN):** classifies cases by assigning the class of similar known cases. The "k" in KNN references the number of cases (neighbors) to consider when assigning a class, and it must be found by testing different values. Given that KNN uses distance metrics to compute nearest neighbors and that each variable is in different scales, it is necessary to scale and center the data prior to fitting the model (Cover and Hart, 1967; Lantz, 2019).
- **Logistic regression:** essentially adapts continuous regression predictions to categorical outcomes (Cramer, 2004; Walker and Duncan, 1967).
- **Decision tree with C5.0** algorithm: is an improvement on decision trees for classification (Quinlan, 2014; Quinlan, 1996).

- **Random fores**: is made of decision trees. Each tree is grown from a random sample of the data and variables, allowing for each tree to grow differently and to better reflect the complexity of the data (Breiman, 2001).

- **Generalized Boosted Model:** (Greenwell et al., 2019; Ridgeway, 2007) implements gradient boosted (Friedman, 2002, 2001), allowing the detection of learning deficiencies and increases model accuracy.

- **Supported vector machine (SVM):** fits hyperplanes into a multidimensional space with the objective of creating homogeneous partitions (Cortes and Vapnik, 1995; Frey and Slate, 1991). The present study tests SVM with linear, radial, and polynomial kernels.

- • **Artificial neural network (ANN):** with multi-layer perception, uses a series of hidden layers and error backpropagation for model training (Rumelhart et al., 1986).

- **Naïve Bayes:** computes class probabilities using Bayes' rule (Weihs et al., 2005).

All models are evaluated using 10×50 k-fold cross validation (10 folds and 50 cycles), providing measures of accuracy. The receiver operating characteristic (ROC) curve is employed to evaluate the ratio of detected true positives while avoiding false positives (Bradley, 1997; Spackman, 1989). The ROC curve allows visually analyzing model performance and calculating the AUC, which ranges from 1 (perfect classifier) to 0.5 (random classifier). AUC ranges of values are usually interpreted as follows: 1 to 0.9: outstanding; 0.9 to 0.8: excellent/good; 0.8 to 0.7: acceptable/fair; 0.7 to 0.6: poor; and 0.6 to 0.5: no discrimination (Lantz, 2019). When analyzing lithic assemblages, the use of thresholds to guarantee true positives and avoid false positives is of special interest. The use of decision thresholds and derived measures of accuracy (ROC curve and AUC) can be especially useful in lithic analysis since it is expected that products from initial reduction stages are morphologically similar independent of the knapping method. It is expected that these products show a higher mixture between methods and have lower probability values. The use of thresholds better indicates the accuracy of a model taking into account these probability values.

The development of the present study was done using R version 4.1.1 in IDE RStudio version 2021.09.0 (R. C. Team, 2019; Rs. Team, 2019). The management of the data and graphs was done using the tidyverse package (Wickham et al., 2019). The training of LDA and KNN was done with MASS (Wright and Ziegler, 2017). The training of SVM was done using the e1071 package (Karatzoglou et al., 2006, 2004). The RSNNS (Bergmeir and Benítez, 2012) package was employed to train multi-layer ANN with backpropagation. The klaR package was employed to train the naïve Bayes classifier (Weihs et al., 2005). The k-fold cross validation of all models, precision metrics, and confusion matrix were obtained using the caret package (Kuhn, 2008). Machine learning models also provide insights into variable importance for classification. The caret package was employed to extract variable importance after each k-fold cross validation.

2.4 Performance of procrustes, PCA and model training

The following line of code performs procrustes alignment and superimposition using the **Morpho** package (Schlager, 2017). Aligned coordinates are extracted and stored as a data frame named **LM.DF**.

```
# Procrustes alignment
proc <- Morpho::ProcGPA(Flakes_LM,
                CSinit = TRUE,
                silent = FALSE)

# Extract coordinates
Proc.Rot <- proc$rotated
LM.DF <- data.frame(matrix(Proc.Rot, nrow = length(filenames), byrow = TRUE))
```

The following line of code performs Principal Components Analysis (PCA) on the set of aligned coordinates stored in the LM.DF data frame. Summary provides proportion and cumulative proportion of variance explained by the 25 first principal components which add up to 95% of variance.

```
# PCA on coordinates
pca <- prcomp(LM.DF, scale. = TRUE)
summary(pca)$importance[1:3, 1:25]
```

```
##                             PC1      PC2      PC3      PC4      PC5      PC6
## Standard deviation     18.05288 16.62783 12.83087 10.83128 10.42072 8.299316
## Proportion of Variance  0.21385  0.18142  0.10803  0.07698  0.07125 0.045200
## Cumulative Proportion   0.21385  0.39527  0.50330  0.58028  0.65153 0.696730
##                             PC7      PC8      PC9     PC10     PC11     PC12
## Standard deviation     7.73039 7.439897 6.710911 6.173021 5.368746 4.773021
## Proportion of Variance 0.03921 0.036320 0.029550 0.025000 0.018910 0.014950
## Cumulative Proportion  0.73594 0.772260 0.801810 0.826810 0.845730 0.860670
##                            PC13    PC14     PC15     PC16    PC17    PC18
## Standard deviation     4.562145 4.44228 3.803028 3.750857 3.54599 3.23142
## Proportion of Variance 0.013660 0.01295 0.009490 0.009230 0.00825 0.00685
## Cumulative Proportion  0.874330 0.88728 0.896770 0.906000 0.91425 0.92110
##                            PC19    PC20     PC21     PC22     PC23    PC24
## Standard deviation     2.956198 2.70170 2.649925 2.516422 2.466077 2.38239
## Proportion of Variance 0.005730 0.00479 0.004610 0.004160 0.003990 0.00372
## Cumulative Proportion  0.926840 0.93163 0.936240 0.940390 0.944380 0.94811
##                            PC25
## Standard deviation     2.327281
## Proportion of Variance 0.003550
## Cumulative Proportion  0.951660
```

Once PCA is performed, values of each of the 25 first PC's can be extracted for each backed flake. Additionally it is necessary to store the PC values along with each backed flake ID. Knapping method is documented for each of the experimental cores and can be added using the `case_when()` function.

```
# Store PCA values in a dataframe and add ID's
PCA_Coord <- as.data.frame(pca$x)
PCA_Coord$ID <- filenames
PCA_Coord$Core <- str_sub(PCA_Coord$ID, end = 2)

# Set the core to which they belong and strategy
PCA_Coord <- PCA_Coord %>% mutate(
  Strategy = case_when(Core == "B2" | Core == "B3" |
              Core == "B4" | Core == "B5" |Core == "B6" ~ "Discoid",
            Core == "B7" | Core == "B8" |Core == "B9" | Core == "Le" ~ "Levallois" ))

# Set strategy as factor or varImp will not work
PCA_Coord$Strategy <- factor(PCA_Coord$Strategy)
```

The resulting `PCA_Coord` data frame haves 25 numeric variables (values of the 25 first PC) along with artifact ID and associated core knapping strategy. This allows to train the models to predict knapping strategy `"Strategy"` based on the values of the 25 first PC. Here, the training of the models is done in three steps:

1) Set the formula.

2) Set the training control and validation method.

3) Train the models using the formula and validation method.

```
# Set formula
frmla <- as.formula(
  paste("Strategy", paste(colnames(PCA_Coord[,1:25]), collapse = " + "), sep = " ~ "))

# Set cross validation
trControl <- trainControl(method  = "repeatedcv",
                          verboseIter = TRUE,
                          number  = 10,
                          repeats = 50,
                          savePredictions = "final",
                          classProbs = TRUE)
```

```
# LDA model
set.seed(123)
fit.LDA <- caret::train(frmla,
                        PCA_Coord,
                        method = "lda",
                        preProc = c("center", "scale"),
                        trControl = trControl)

# KNN model
set.seed(123)
KNN.model <- caret::train(
  frmla,
  PCA_Coord,
  method = "knn",
  preProc = c("center", "scale"),
  trControl = trControl,
  tuneGrid = expand.grid(k = seq(1, 15, 1))
)

# Logistic regression model
set.seed(123)
logmod <- caret::train(frmla,
                       PCA_Coord,
                       method = "glm",
                       family = "binomial",
                       preProc = c("center", "scale"),
                       trControl = trControl)

# SVM linear
set.seed(123)
SVM_Linear <- train(frmla,
                    PCA_Coord,
                    method = "svmLinear",
                    preProcess = c("center","scale"),
                    trControl = trControl,
                    tuneGrid = expand.grid(C = seq(0.01, 3, length = 20)),
                    metric = "Accuracy",
                    importance = 'impurity')
```

```
# SVM Radial
set.seed(123)
SVM_Radial <- train(frmla,
                    PCA_Coord,
                    method = "svmRadial",
                    preProcess = c("center","scale"),
                    trControl = trControl,
                    tuneGrid =
                      expand.grid(C = seq(0.01, 3, length = 20),
                                  sigma = seq(0.0001, 1, length = 20)),
                    metric = "Accuracy",
                    importance = 'impurity')

# SVM Poly
set.seed(123)
SVM_Poly <- train(frmla,
                  PCA_Coord,
                  method = "svmPoly",
                  preProcess = c("center","scale"),
                  trControl = trControl,
                  metric = "Accuracy",
                  tuneGrid =
                    expand.grid(C = seq(0.01, 3, length = 15),
                                scale = seq(0.001, 1, length = 15),
                                degree = as.integer(seq(1, 3, 1))),
                  importance = 'impurity')

# Random Forest
best_tune <- data.frame(
  mtry = numeric(0),
  Num_Trees = numeric(0),
  Split_Rule = character(0),
  Precision = numeric(0),
  Node.Size = numeric(0))

my_seq <- seq(350, 700, 25)
set.seed(123)
for (x in my_seq){
  RF_Model <- train(frmla,
                    PCA_Coord,
                    method = "ranger",
                    trControl = trControl,
                    tuneGrid =
                      expand.grid(.mtry = seq(1, 10, 1),
                                  .min.node.size = seq(1, 6, 1),
                                  .splitrule = c("gini", "extratrees")),
                    metric = "Accuracy",
                    importance = 'impurity')

  Bst_R <- data.frame(
    mtry = RF_Model$bestTune[[1]],
    Num_Trees = x,
    Split_Rule = RF_Model$bestTune[[2]],
```

```
    Precision = max(RF_Model$results[[4]]),
    Node.Size = RF_Model$bestTune[[3]]
  )

  best_tune <- rbind(best_tune, Bst_R)

  Bst_R <- c()
}

# Best tune
# mtry = 7; 550 trees split_Rule = extratrees; min.nod.size = 6
set.seed(123)
RF_Model <- train(
  frmla,
  PCA_Coord,
  method = "ranger",
  trControl = trControl,
  tuneGrid = expand.grid(
    .mtry = 7,
    .min.node.size = 6,
    .splitrule = "extratrees"),
  num.trees = 550,
  metric = "Accuracy",
  importance = 'impurity')

# Boosted tree
set.seed(123)
Boost_Tree <- train(frmla,
                    PCA_Coord,
                    method = "gbm",
                    trControl = trControl,
                    metric = "Accuracy",
                    tuneGrid =
                      expand.grid(
                        n.trees = seq(from = 300, to = 700, by = 50),
                        interaction.depth = seq(from = 1, to = 10, length.out = 5),
                        shrinkage = 0.1,
                        n.minobsinnode = as.integer(seq(1, 10, length = 5))))

# Multilayer ANN
set.seed(123)
mlp_Mod = train(frmla,
                  PCA_Coord,
                  method = "mlpML",
                  preProc =  c('center', 'scale'),
                  trControl = trControl,
                  tuneGrid =
                    expand.grid(
                      layer1 = c(1:8),
                      layer2 = c(0:8),
                      layer3 = c(0:8)))

# Naive Bayes
```

```
set.seed(123)
NaiB_Model <- train(frmla,
                    PCA_Coord,
                    method = "nb",
                    preProcess = c("scale","center"),
                    trControl = trControl,
                    metric = "Accuracy",
                    lineout = FALSE)

confusionMatrix(NaiB_Model)

# C5.0 Tree
grid <- expand.grid(
  winnow = c(TRUE),
  trials = seq(10, 40, by = 5),
  model = "tree" )

set.seed(123)
C50_Mod <- train(frmla,
                 PCA_Coord,
                 method = "C5.0",
                 trControl = trControl,
                 metric = "Accuracy",
                 importance = 'impurity')
```

3 Results

3.1 PCA and model performance

PCA results show that the 25 first principal components account for 95% of the variance of the dataset with PC1 accounting for 21.39% of variance and PC25 accounting for 0.36% of variance. This is an important reduction from the original number of variables (1524) and substantially lower than the sample (139). The following table presents the performance metrics for each of the models. In general, all models performed with accuracy values higher than 0.7 with the exception of KNN, Naïve Bayes, and the decision tree with C5.0 algorithm. When considering the two measures of overall model performance (F1 and accuracy), SVM with polynomial kernel presents the highest performance values (F1 = 0.75 and accuracy = 0.757). Additionally, SVM with polynomial kernel also provides the highest values of precision.

```
# Data frame of models performance
data.frame(
  Model = c("LDA", "KNN", "Log. Reg.", "SVML", "SVMP", "SVMR",
            "C5.0", "Rand. Forest", "Boost Tree", "Baïve Bayes",
            "ANN") %>%
    cbind(
  data.frame(
 rbind(
   round(confusionMatrix(fit.LDA$pred$pred, fit.LDA$pred$obs)[[4]][c(1,2,5,7,11)],3),
   round(confusionMatrix(KNN.model$pred$pred, KNN.model$pred$obs)[[4]][c(1,2,5,7,11)],3),
   round(confusionMatrix(logmod$pred$pred, logmod$pred$obs)[[4]][c(1,2,5,7,11)],3),
   round(confusionMatrix(SVM_Linear$pred$pred, SVM_Linear$pred$obs)[[4]][c(1,2,5,7,11)],3),
   round(confusionMatrix(SVM_Poly$pred$pred, SVM_Poly$pred$obs)[[4]][c(1,2,5,7,11)],3),
   round(confusionMatrix(SVM_Radial$pred$pred, SVM_Radial$pred$obs)[[4]][c(1,2,5,7,11)],3),
```

```
  round(confusionMatrix(C50_Mod$pred$pred, C50_Mod$pred$obs)[[4]][c(1,2,5,7,11)],3),
  round(confusionMatrix(RF_Model$pred$pred, RF_Model$pred$obs)[[4]][c(1,2,5,7,11)],3),
  round(confusionMatrix(Boost_Tree$pred$pred, Boost_Tree$pred$obs)[[4]][c(1,2,5,7,11)],3),
  round(confusionMatrix(NaiB_Model$pred$pred, NaiB_Model$pred$obs)[[4]][c(1,2,5,7,11)],3),
  round(confusionMatrix(mlp_Mod$pred$pred, mlp_Mod$pred$obs)[[4]][c(1,2,5,7,11)],3)))
 ))
```

```
##         Model.. Model.Sensitivity Model.Specificity Model.Precision Model.F1
## 1           LDA             0.682             0.767           0.748    0.713
## 2           KNN             0.333             0.888           0.751    0.461
## 3     Log. Reg.             0.699             0.734           0.727    0.713
## 4          SVML             0.684             0.798           0.774    0.726
## 5          SVMP             0.723             0.790           0.778    0.750
## 6          SVMR             0.733             0.716           0.723    0.728
## 7          C5.0             0.660             0.657           0.661    0.661
## 8  Rand. Forest             0.707             0.742           0.735    0.721
## 9    Boost Tree             0.725             0.739           0.738    0.732
## 10  Baïve Bayes             0.670             0.725           0.712    0.690
## 11          ANN             0.695             0.718           0.714    0.704
##    Model.Balanced.Accuracy
## 1                    0.724
## 2                    0.610
## 3                    0.717
## 4                    0.741
## 5                    0.757
## 6                    0.724
## 7                    0.659
## 8                    0.724
## 9                    0.732
## 10                   0.697
## 11                   0.706
```

SVM with polynomial kernel is closely followed by SVM with a linear kernel, which presents the second highest value of accuracy (0.741), the fourth highest value of F1 (0.726), and the second-highest value of precision (0.774). Outside SVM with different kernels, the boosted trees also presents high values of accuracy (0.732), F1 (0.732), and precision (0.738). KNN presented the lowest values on the general performance metrics, with an accuracy value of 0.61 and a very low F1 score (0.461). KNN does seem to present high values of precision (0.751) and specificity (0.888) although these are clearly the result of a sensitivity (0.333) lower than the no-information ratio (0.504).

```
# LDA
temp <- pROC::roc(fit.LDA$pred$obs, fit.LDA$pred$Levallois)
Roc_Curve <- tibble(temp$specificities, temp$sensitivities)
Roc_Curve$Model <- "LDA"

# KNN
temp <- pROC::roc(KNN.model$pred$obs, KNN.model$pred$Levallois)
temp <- cbind(tibble(temp$specificities, temp$sensitivities),
              Model = "KNN")
Roc_Curve <- rbind(Roc_Curve, temp)

# Log
temp <- pROC::roc(logmod$pred$obs, logmod$pred$Levallois)
```

```
temp <- cbind(tibble(temp$specificities, temp$sensitivities),
              Model = "Log. Reg.")
Roc_Curve <- rbind(Roc_Curve, temp)

# SVML
temp <- pROC::roc(SVM_Linear$pred$obs, SVM_Linear$pred$Levallois)
temp <- cbind(tibble(temp$specificities, temp$sensitivities),
              Model = "SVML")
Roc_Curve <- rbind(Roc_Curve, temp)

# SVMP
temp <- pROC::roc(SVM_Poly$pred$obs, SVM_Poly$pred$Levallois)
temp <- cbind(tibble(temp$specificities, temp$sensitivities),
              Model = "SVMP")
Roc_Curve <- rbind(Roc_Curve, temp)

# SVMR
temp <- pROC::roc(SVM_Radial$pred$obs, SVM_Radial$pred$Levallois)
temp <- cbind(tibble(temp$specificities, temp$sensitivities),
              Model = "SVMR")
Roc_Curve <- rbind(Roc_Curve, temp)

# C5.0
temp <- pROC::roc(C50_Mod$pred$obs, C50_Mod$pred$Levallois)
temp <- cbind(tibble(temp$specificities, temp$sensitivities),
              Model = "C5.0")
Roc_Curve <- rbind(Roc_Curve, temp)

# rf
temp <- pROC::roc(RF_Model$pred$obs, RF_Model$pred$Levallois)
temp <- cbind(tibble(temp$specificities, temp$sensitivities),
              Model = "Rand. Forest")
Roc_Curve <- rbind(Roc_Curve, temp)

# Boosted tree
temp <- pROC::roc(Boost_Tree$pred$obs, Boost_Tree$pred$Levallois)
temp <- cbind(tibble(temp$specificities, temp$sensitivities),
              Model = "Boost Tree")
Roc_Curve <- rbind(Roc_Curve, temp)

# Boosted tree
temp <- pROC::roc(NaiB_Model$pred$obs, NaiB_Model$pred$Levallois)
temp <- cbind(tibble(temp$specificities, temp$sensitivities),
              Model = "Naïve Bayes")
Roc_Curve <- rbind(Roc_Curve, temp)

# Boosted tree
temp <- pROC::roc(mlp_Mod$pred$obs, mlp_Mod$pred$Levallois)
temp <- cbind(tibble(temp$specificities, temp$sensitivities),
              Model = "ANN")
Roc_Curve <- rbind(Roc_Curve, temp)
rm(temp)
```

```
aucs <- c(
  paste0("LDA (", round(pROC::auc(fit.LDA$pred$obs, fit.LDA$pred$Levallois),2) ,")"),
  paste0("KNN (", round(pROC::auc(KNN.model$pred$obs, KNN.model$pred$Levallois),2) ,")"),
  paste0("Logistic (", round(pROC::auc(logmod$pred$obs, logmod$pred$Levallois),2) ,")"),
  paste0("SVM Linear (", round(pROC::auc(SVM_Linear$pred$obs, SVM_Linear$pred$Levallois),2) ,")"),
  paste0("SVM Poly (", round(pROC::auc(SVM_Poly$pred$obs, SVM_Poly$pred$Levallois),2) ,")"),
  paste0("SVM Radial (", round(pROC::auc(SVM_Radial$pred$obs, SVM_Radial$pred$Levallois),2) ,")"),
  paste0("C5.0 (", round(pROC::auc(C50_Mod$pred$obs, C50_Mod$pred$Levallois),2) ,")"),
  paste0("Rand. Forest (", round(pROC::auc(RF_Model$pred$obs, RF_Model$pred$Levallois),2) ,")"),
  paste0("Boosted. Tree (", round(pROC::auc(Boost_Tree$pred$obs, Boost_Tree$pred$Levallois),2) ,")"),
  paste0("Naïve Bayes (", round(pROC::auc(NaiB_Model$pred$obs, NaiB_Model$pred$Levallois),2) ,")"),
  paste0("ANN (", round(pROC::auc(mlp_Mod$pred$obs, mlp_Mod$pred$Levallois),2) ,")"))

Roc_Curve %>%
  ggplot(aes(`temp$specificities`, `temp$sensitivities`,
             color = Model), alpha = 0.7) +
  geom_line(size = 1.01) +
  scale_x_continuous(trans = "reverse") +
  coord_fixed() +
  theme_light() +
  xlab("Specificities") +
  ylab("Sensitivities") +
  geom_abline(intercept = 1, slope = 1)  +
  scale_color_brewer(palette = "Paired",
                     breaks = c("LDA", "KNN", "Log. Reg.",
                                "SVML", "SVMP", "SVMR", "C5.0",
                                "Rand. Forest", "Boost Tree",
                                "Naïve Bayes", "ANN"),
                     labels = aucs) +
  labs(colour = "Model (AUC)") +
  theme(
    axis.title = element_text(size = 11, color = "black", face = "bold"),
    axis.text = element_text(size = 10, color = "black"),
    legend.title = element_text(face = "bold"))
```

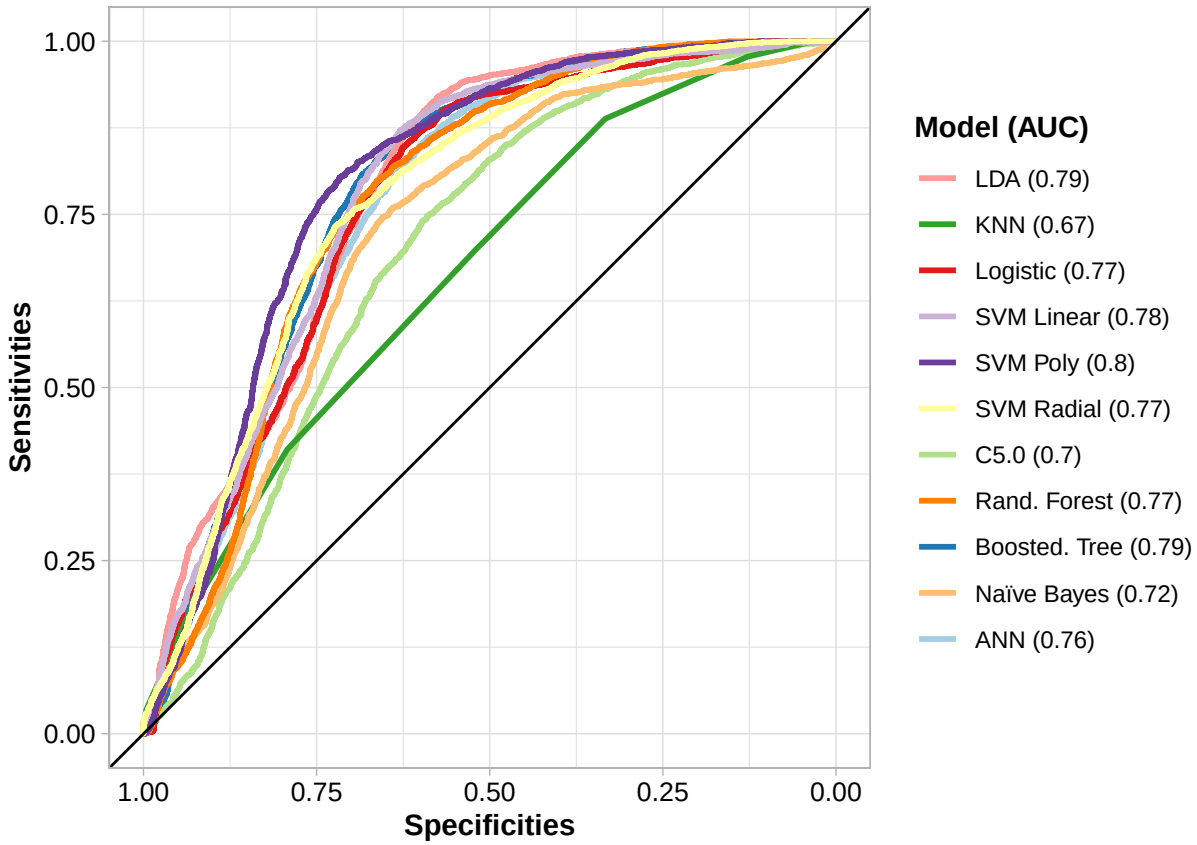

The evaluation of the models through the ROC curve and AUC shows that most models present acceptable/fair (0.8–0.7) values. Again, KNN presents the lowest AUC (0.67), a poor value. SVM with polynomial kernel presents the highest AUC value (0.799) and is thus very close to being an excellent/good model (0.9 to 0.8). The optimal probability threshold values from the SVM with polynomial kernel are 0.501 for discoidal and 0.491 for Levallois. The general performance metrics (F1 and accuracy) and AUC values indicate that SVM with polynomial kernel is the best model. The evaluation of SVM with the polynomial kernel confusion matrix shows a very good distribution along the diagonal axis, with the correct identification of Levallois products being slightly higher than the correct identification of discoidal products. The directionality of confusions shows that for the SVM with polynomial kernel, it is more common to mistake discoidal backed products for Levallois rather than mistaking Levallois backed products for those from discoidal reduction sequences.

```
# Confusion matrix
SVM_Poly.Confx <- confusionMatrix(SVM_Poly)$table

SVM_Poly.Confx <- reshape2::melt(SVM_Poly.Confx)

SVM_Poly.Confx$Prediction <- factor(SVM_Poly.Confx$Prediction,
                                    levels = c(
                                      "Discoid", "Levallois"))
SVM_Poly.Confx$Reference <- factor(SVM_Poly.Confx$Reference,
                                   levels = c(
                                     "Levallois", "Discoid"))

SVM_Poly.Confx %>%
  ggplot(aes(Reference, Prediction, fill = value)) +
```

```
  geom_tile(alpha = 0.75) +
  geom_text(aes(label = round(value, 2)), size = 3) +
  scale_fill_gradient(low = "white", high = "blue")  +
  scale_x_discrete(position = "top") +
  theme_bw() +
  coord_fixed() +
  theme(legend.position = "none",
        axis.title = element_text(size = 8, color = "black", face = "bold"),
        axis.text = element_text(size = 7.5, color = "black"),
        title = element_text(size = 8, color = "black", face = "bold"))
```

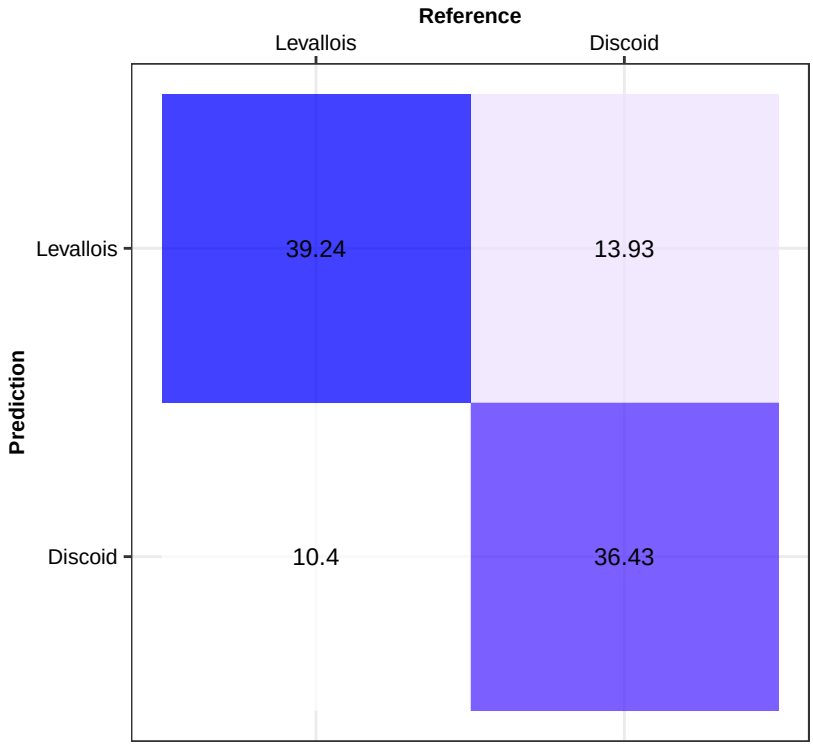

3.2 PC Importance

The following figure presents the PC importance for the discrimination of knapping method according to SVM with polynomial kernel model. The PC importance shows that PC3 clearly stands out in importance for the discrimination of discoidal and Levallois backed products. PC3 only accounts for 10.8% of the variance but presents the maximum scaled importance. PC1, which represents 21.39% of the variance, is the second most important variable, with a score of 46.64, although far from PC3. PC8, which represents only 3.63% of the variance, is the third most important variable for the SVM with polynomial kernel model.

```
# Data frame of PC importance
tibble(
  PC = rownames(varImp(SVM_Poly, sale = TRUE)$importance),
  Importance = varImp(SVM_Poly, sale = TRUE)$importance[, 1]) %>%

  top_n(15, Importance) %>%
# and plot
```

```
  ggplot(aes(Importance, reorder(PC, Importance), fill = Importance)) +
  geom_bar(stat= "identity", position = "dodge") +
  geom_text(aes(label = round(Importance, 2)),
            position = position_stack(vjust = 0.5), size = 2) +
  scale_fill_gradient(low = "red", high = "blue") +
  guides(fill = "none") +
  coord_flip() +
  ylab(NULL) +
  theme_light() +
  theme(
    axis.text.y = element_text(color = "black", size = 7),
    axis.text.x = element_text(color = "black", size = 7),
    axis.title.x = element_text(color = "black", size = 9),
    axis.title.y = element_text(color = "black", size = 9))
```

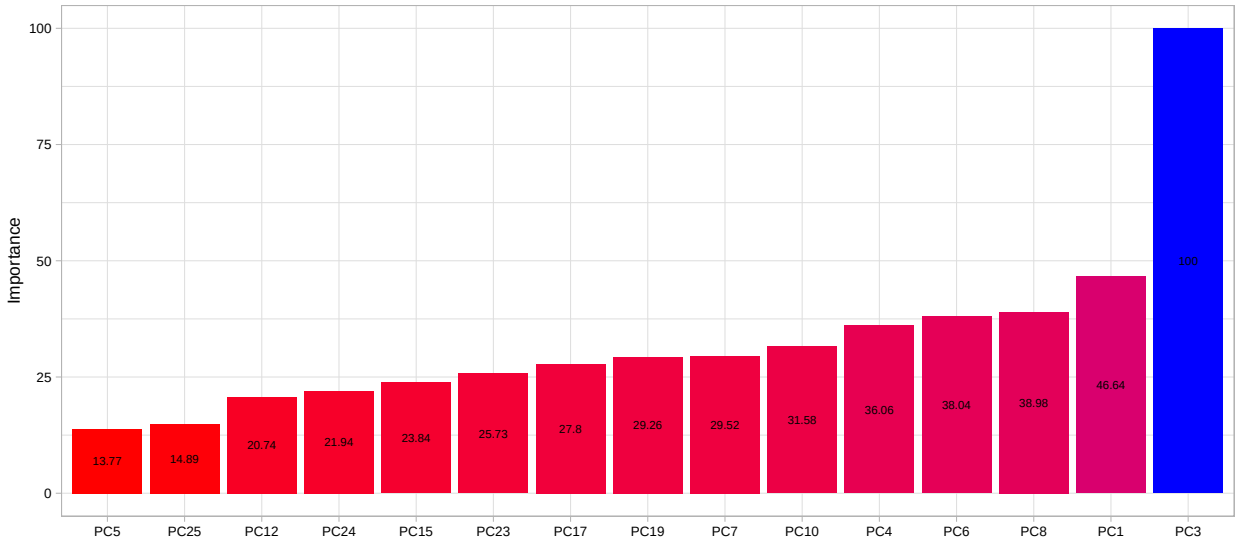


```
#PC biplots
ggpubr::ggarrange(
(PCA_Coord %>% ggplot(aes(PC3, PC1, fill = Strategy)) +
  geom_vline(xintercept = 0, alpha = 0.7, linetype = "dashed") +
  geom_hline(yintercept = 0, alpha = 0.7, linetype = "dashed") +
  stat_ellipse(geom = "polygon", alpha = 0.2, aes(fill = Strategy)) +
  geom_point(aes(color = Strategy)) +
  xlab(paste0("PC3 (", round((summary(pca)$importance[2,3])*100, 2), "%)")) +
  ylab(paste0("PC1 (", round((summary(pca)$importance[2,1])*100, 2), "%)")) +
  ggsci::scale_fill_aaas() +
  ggsci::scale_color_aaas() +
  theme_light() +
  theme(
    axis.text.y = element_text(color = "black", size = 7),
    axis.text.x = element_text(color = "black", size = 7),
    axis.title.x = element_text(color = "black", size = 9),
    axis.title.y = element_text(color = "black", size = 9),
    legend.position = "bottom")),
```

```
(PCA_Coord %>% ggplot(aes(PC3, PC8, fill = Strategy)) +
  geom_vline(xintercept = 0, alpha = 0.7, linetype = "dashed") +
  geom_hline(yintercept = 0, alpha = 0.7, linetype = "dashed") +
  stat_ellipse(geom = "polygon", alpha = 0.2, aes(fill = Strategy)) +
  geom_point(aes(color = Strategy)) +
  xlab(paste0("PC3 (", round((summary(pca)$importance[2,3])*100, 2), "%)")) +
  ylab(paste0("PC8 (", round((summary(pca)$importance[2,8])*100, 2), "%)")) +
  ggsci::scale_fill_aaas() +
  ggsci::scale_color_aaas() +
  theme_light() +
  theme(
    axis.text.y = element_text(color = "black", size = 7),
    axis.text.x = element_text(color = "black", size = 7),
    axis.title.x = element_text(color = "black", size = 9),
    axis.title.y = element_text(color = "black", size = 9),
    legend.position = "bottom")),
ncol = 2,
common.legend = TRUE,
legend = "bottom",
align = "h")
```

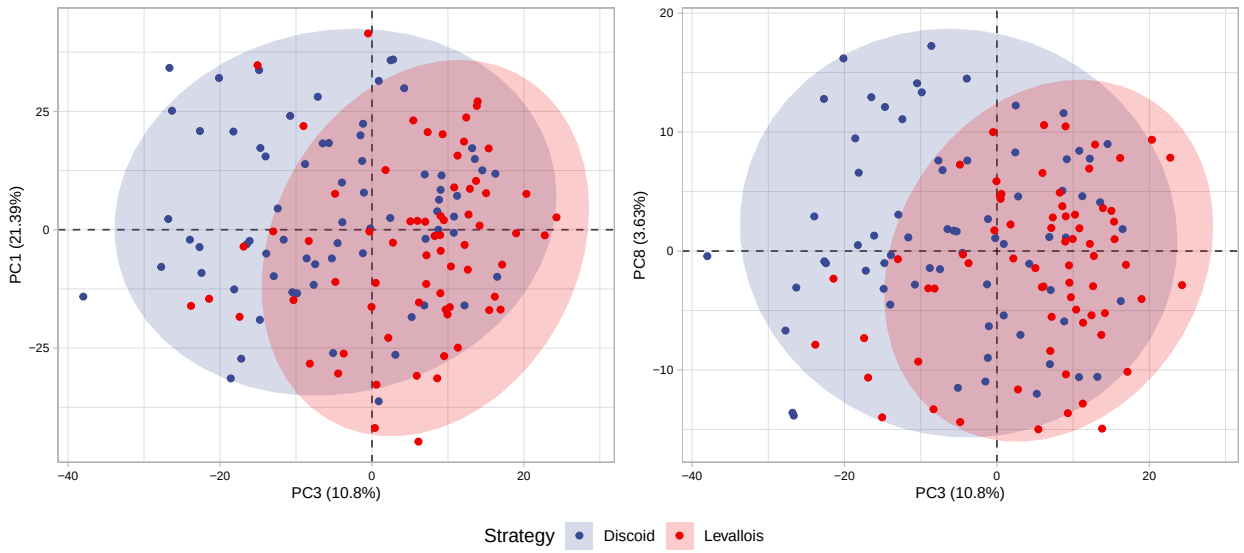

The effect of PC3 on identifying backed products from the two knapping methods is especially notable in the a biplot distribution. The above figure presents a biplot distribution of the data between PC3 and the following two most important variables. In both cases, backed flakes detached from Levallois recurrent centripetal cores tend to be clustered in the positive values of PC3, whereas they show a wider distribution, usually centered on the 0 value, for PCs 1 and 8. Backed flakes from discoidal reduction sequences show a wider distribution although the center is in the negative and 0 values of PC3. Although the combination of PC3 with PC1 and PC8 shows an overlapping of the confidence ellipsis, differentiation between both groups can be observed.

The following figure presents a biplot distribution of the data when the second (PC1), third (PC8), and fourth (PC6) most important variables are employed. The biplot from the combination of these variables shows much more consistent overlapping for the different combinations of PC1, PC8, and PC6.

```
ggpubr::ggarrange(
(PCA_Coord %>% ggplot(aes(PC1, PC8, fill = Strategy)) +
```

```
  geom_vline(xintercept = 0, alpha = 0.7, linetype = "dashed") +
  geom_hline(yintercept = 0, alpha = 0.7, linetype = "dashed") +
  stat_ellipse(geom = "polygon", alpha = 0.2, aes(fill = Strategy)) +
  geom_point(aes(color = Strategy)) +
  xlab(paste0("PC1 (", round((summary(pca)$importance[2,1])*100, 2), "%)")) +
  ylab(paste0("PC8 (", round((summary(pca)$importance[2,8])*100, 2), "%)")) +
  ggsci::scale_fill_aaas() +
  ggsci::scale_color_aaas() +
  theme_light() +
  theme(
    axis.text.y = element_text(color = "black", size = 7),
    axis.text.x = element_text(color = "black", size = 7),
    axis.title.x = element_text(color = "black", size = 9),
    axis.title.y = element_text(color = "black", size = 9),
    legend.position = "bottom")),

(PCA_Coord %>% ggplot(aes(PC1, PC6, fill = Strategy)) +
  geom_vline(xintercept = 0, alpha = 0.7, linetype = "dashed") +
  geom_hline(yintercept = 0, alpha = 0.7, linetype = "dashed") +
  stat_ellipse(geom = "polygon", alpha = 0.2, aes(fill = Strategy)) +
  geom_point(aes(color = Strategy)) +
  xlab(paste0("PC1 (", round((summary(pca)$importance[2,1])*100, 2), "%)")) +
  ylab(paste0("PC6 (", round((summary(pca)$importance[2,6])*100, 2), "%)")) +
  ggsci::scale_fill_aaas() +
  ggsci::scale_color_aaas() +
  theme_light() +
  theme(
    axis.text.y = element_text(color = "black", size = 7),
    axis.text.x = element_text(color = "black", size = 7),
    axis.title.x = element_text(color = "black", size = 9),
    axis.title.y = element_text(color = "black", size = 9),
    legend.position = "bottom")),
ncol = 2,
common.legend = TRUE,
legend = "bottom",
align = "h")
```

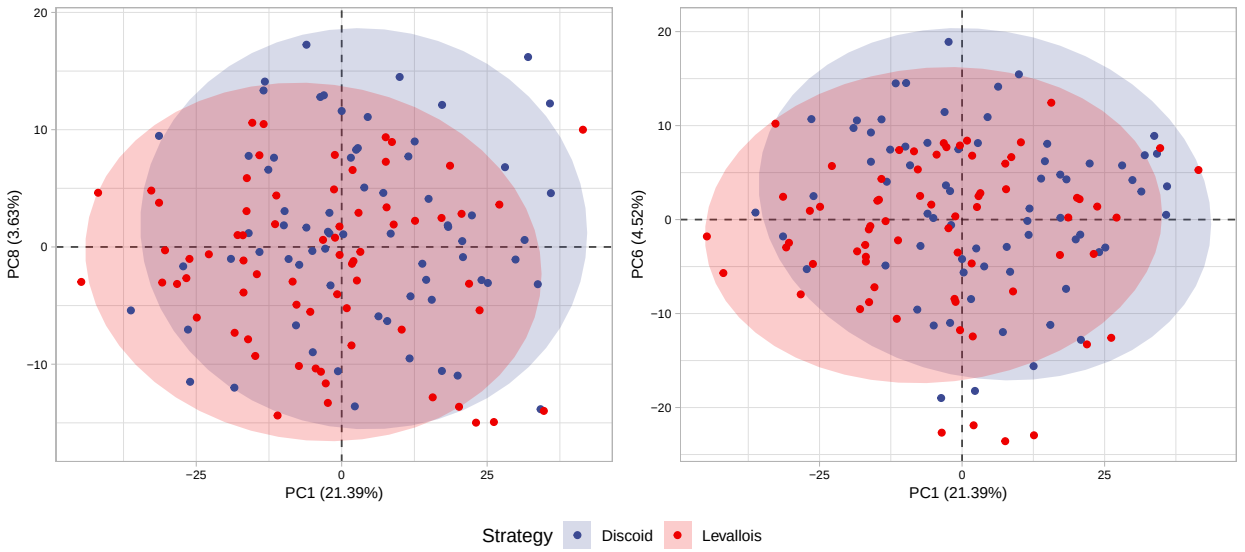

Prior to perform multiple linear regression to predict PC values based on flake metric features it is necessary to join both data sets (the one containing PC values and the one containing attribute analysis values). The following code load the data from recorded attributes and performs a `left_join()` to match PC and attribute values according to flake ID.

```
# Read in attribute dataset
Att <- read.csv("Data/Attributes data.csv")

# Left joined with the attribute database
PCA_Coord <- left_join(PCA_Coord, Att, by = "ID")

# Compute ratios
PCA_Coord <- PCA_Coord %>%
  mutate(Lam.Ind = LENGHT/WIDTH,
         Caren.Ind = case_when(
           LENGHT < WIDTH ~ LENGHT/MAXTHICK,
           LENGHT > WIDTH ~ WIDTH/MAXTHICK,
           LENGHT == WIDTH ~ WIDTH/MAXTHICK),
         Flat_Ind = (WIDTH*LENGHT)/MAXTHICK,
         Flak.Surface = WIDTH*LENGHT,
         W.to.Thic = WIDTH/MAXTHICK)
```

Multiple linear regression for the prediction of PC3 indicates that the best correlation is obtained when the interaction of IPA and the ratio of flake width to thickness is employed ($p < 0.001$, adjusted $r^2 = 0.65$). The coefficient of the interaction between the ratio of width to thickness and IPA is 0.17, whereas the coefficient of IPA is -0.77. This indicates that as the IPA becomes more open as the values of PC3 decrease. The ratio of flake width to thickness offers a counterintuitive coefficient of -12.79. The signal of this coefficient is opposite to that obtained from a linear regression where the values of the ratio of flake width to thickness are employed to predict PC3 values ($p < 0.001$; $r^2 = 0.6$; coefficient = 6.46). The reversed signal obtained from the interaction can be considered the result of Simpson's paradox (Simpson, 1951). The high correlation between the carenated index and the ratio of flake width to thickness ($p < 0.001$; $r^2 = 0.9$) indicates that PC3 captures relative flake thinness to thickness although it regresses better with the ratio of width to thickness. In general, thin flakes with an IPA close to 90^o will have high positive PC3 values, whereas thick flakes with open IPA will have negative values.

```r
# Best predictors fort PC3
summary(lm(PC3 ~ W.to.Thic*IPA, PCA_Coord))
```

```
##
## Call:
## lm(formula = PC3 ~ W.to.Thic * IPA, data = PCA_Coord)
##
## Residuals:
##      Min       1Q   Median       3Q      Max
## -22.4659  -4.6226  -0.2159   4.8543  21.1260
##
## Coefficients:
##                Estimate Std. Error t value Pr(>|t|)
## (Intercept)    62.02025   17.75208   3.494 0.000645 ***
## W.to.Thic     -12.79366    4.22008  -3.032 0.002917 **
## IPA            -0.77034    0.15657  -4.920 2.48e-06 ***
## W.to.Thic:IPA   0.17362    0.03855   4.503 1.43e-05 ***
## ---
## Signif. codes:  0 '***' 0.001 '**' 0.01 '*' 0.05 '.' 0.1 ' ' 1
##
## Residual standard error: 7.597 on 135 degrees of freedom
## Multiple R-squared:  0.657,  Adjusted R-squared:  0.6494
## F-statistic: 86.21 on 3 and 135 DF,  p-value: < 2.2e-16
```

```r
# Correlation between Carenated index and ratio of width to thickness
summary(lm(Caren.Ind ~ W.to.Thic, PCA_Coord))
```

```
##
## Call:
## lm(formula = Caren.Ind ~ W.to.Thic, data = PCA_Coord)
##
## Residuals:
##      Min       1Q   Median       3Q      Max
## -1.74506 -0.15789  0.09566  0.26291  0.86470
##
## Coefficients:
##             Estimate Std. Error t value Pr(>|t|)
## (Intercept)  0.21885    0.10253   2.134   0.0346 *
## W.to.Thic    0.86108    0.02486  34.632   <2e-16 ***
## ---
## Signif. codes:  0 '***' 0.001 '**' 0.01 '*' 0.05 '.' 0.1 ' ' 1
##
## Residual standard error: 0.4477 on 137 degrees of freedom
## Multiple R-squared:  0.8975, Adjusted R-squared:  0.8967
## F-statistic:  1199 on 1 and 137 DF,  p-value: < 2.2e-16
```

An analysis of PC3 values according to group shows that backed products from Levallois recurrent centripetal methods tend to have higher values (mean = 5.47) with a slightly lower standard deviation. Backed products detached from discoidal cores, alternatively, tend to have lower values (mean = -5.20) and a slightly higher standard deviation (12.74).

```r
 # Descriptive statistics of PC3
data.frame(
  PCA_Coord %>%
    group_by(Strategy.y) %>%
    summarise(
      Min = min(PC3),
      `5th Perc` = quantile(PC3, 0.05),
      `1st quantile` = quantile(PC3, 0.25),
      Mean = mean(PC3),
      Meadian = quantile(PC3, 0.5),
      `3rd quantile` = quantile(PC3, 0.75),
      `95 Perc` = quantile(PC3, 0.95),
      Max = max(PC3),
      SD = sd(PC3)))
```

```
##   Strategy.y       Min X5th.Perc X1st.quantile      Mean   Meadian
## 1    Discoid -38.00047 -26.50603    -14.741836 -5.388529 -5.200406
## 2  Levallois -23.82052 -16.16213      0.385224  5.466624  8.588994
##   X3rd.quantile X95.Perc      Max       SD
## 1      4.984441  13.3835 16.49057 12.74186
## 2     12.411823  18.2428 24.29432 10.44742
```

Multiple linear regression for the prediction of PC1 values shows a moderate correlation when the elongation index and carenated index are employed as predictors ($p < 0.001$; adjusted $r^2 = 0.63$). The elongation index presents the highest significance and the highest estimate value (-39.27), whereas the carenated index presents an estimate value of -4.26. The negative and high value of the estimate for the elongation index indicates that as the elongation tendency of a product increases (becoming longer relative to its width), the values of PC1 will decrease while all other variables remain constant. The negative estimate of the carenated index also indicates that as a product becomes thinner, the values of PC1 will decrease. Thus, the positive values of PC1 represent thick products with a low elongation.

```r
# Prediction of PC1 values
summary(lm(PC1 ~ Caren.Ind + Lam.Ind, PCA_Coord))
```

```
##
## Call:
## lm(formula = PC1 ~ Caren.Ind + Lam.Ind, data = PCA_Coord)
##
## Residuals:
##     Min      1Q  Median      3Q     Max
## -34.306  -5.736   0.297   8.171  22.534
##
## Coefficients:
##             Estimate Std. Error t value Pr(>|t|)
## (Intercept)  59.0190     4.3058  13.707  < 2e-16 ***
## Caren.Ind    -4.2556     0.6908  -6.161 7.69e-09 ***
## Lam.Ind     -39.2654     2.6099 -15.045  < 2e-16 ***
## ---
## Signif. codes:  0 '***' 0.001 '**' 0.01 '*' 0.05 '.' 0.1 ' ' 1
##
## Residual standard error: 11.02 on 136 degrees of freedom
## Multiple R-squared:  0.633,  Adjusted R-squared:  0.6276
## F-statistic: 117.3 on 2 and 136 DF,  p-value: < 2.2e-16
```

The analysis of PC1 values shows differences between the backed products of the discoidal and Levallois recurrent centripetal methods. On average, backed products from the Levallois recurrent centripetal method will have higher values (mean = 3.75) compared to discoidal products (mean = -3.80). However, an important overlapping of values is evident for products from both reduction methods, with high values of standard deviation in both cases.

```
# Descriptive statistics of PC1
data.frame(
  PCA_Coord %>%
    group_by(Strategy.y) %>%
    summarise(
      Min = min(PC1),
      `5th Perc` = quantile(PC1, 0.05),
      `1st quantile` = quantile(PC1, 0.25),
      Mean = mean(PC1),
      Meadian = quantile(PC1, 0.5),
      `3rd quantile` = quantile(PC1, 0.75),
      `95 Perc` = quantile(PC1, 0.95),
      Max = max(PC1),
      SD = sd(PC1)))
```

```
##   Strategy.y       Min X5th.Perc X1st.quantile      Mean   Meadian
## 1    Discoid -36.23377 -26.25343     -7.711467  3.747729  2.372406
## 2  Levallois -44.75778 -31.17264    -16.301620 -3.802044 -2.736412
##   X3rd.quantile X95.Perc      Max      SD
## 1     16.789563 32.95855 35.95467 17.3134
## 2      7.584384 25.18118 41.46336 18.1138
```

4. Discussion

Our results have shown an accuracy of 0.76 for the differentiation of discoidal and Levallois recurrent centripetal methods on backed products. Additionally, the use of decision thresholds provided an AUC close to 0.8. This degree of accuracy indicates that the quantification of morphological features through geometric morphometrics, along with dimensionality reduction using PCA and machine learning models, can accurately differentiate between the two methods tested. Of the 11 models tested, SVM with polynomial kernel provided the best performance for the discrimination of discoidal and Levallois recurrent centripetal methods in backed artifacts. Moreover, results support the notion that discoidal and recurrent centripetal Levallois are two separate core reduction methods/conceptions.

The first 25 PCs captured 95% of the sample variance. Of these PCs, the highest importance value for the discrimination of knapping methods was obtained by PC3. Multiple linear regression shows that PC3 is moderately correlated with an interaction between IPA and the ratio of flake width to thickness. Thin and wide artifacts with IPA values close to 90º will have higher PC3 values. The examination of biplots and PC3 values shows that backed flakes detached from Levallois recurrent centripetal cores will tend to be thin in relation to the thickness, non-elongated, and have an IPA close to 90º. PC1, which captures elongation tendencies with higher resolution (along with product thickness) also supports this interpretation although higher overlapping exists. The discriminatory power of PC3 appears inherently related to differences in how the volume of cores in the two methods are conceived: non-hierarchized surfaces exploited with secant removals in discoidal reduction while recurrent centripetal Levallois is characterized by sub-parallel removals from a single debitage surface. Additional features for the discrimination of discoidal and Levallois backed products can be found in the edge angles and in the angles of the negatives of the dorsal face towards the detachment surface. In general, it is expected that products detached from Levallois reduction sequences will have more acute edge angles, along with dorsal surface negatives which will be in accordance with flatter

surfaces. Again, these differences in the angles are also inherently related to the differences in how the volume of cores of the two methods are conceived.

These results indicate that there are underlying morphological differences between backed artifacts detached from both methods. These underlying morphological differences can be captured and quantified by geometric morphometrics along with PCA and used by machine learning models for an accurate discrimination of methods.

Several authors have pointed out underlying morphological characteristics that can differentiate backed products detached from Levallois recurrent centripetal and discoidal cores (Boëda et al., 1990; Delpiano et al., 2021; Meignen, 1996; Meignen, 1993; Mourre, 2003). As previously pointed out, one of the features captured by PC3 is the IPA. Products that have an IPA close to 90º have increasing PC3 values, being the case for most Levallois backed flakes. Levallois products having an IPA close to 90º have been described previous to (Kelly, 1954) and after (Boëda, 1995b, 1994, 1993) the technological description of the Levallois flaking system. A recent study employing machine learning models (González-Molina et al., 2020) on attribute analysis have also pointed to the IPA as one of the features allowing differentiation between Levallois recurrent centripetal and Discoid products.

Delpiano et al. (2021) focused on the general morphology of Discoid and Levallois backed products, stating that the latter tend to be thinner with subparallel and rectilinear edges and a higher elongation. The interpretation of PC3 in the present study also identifies backed products from Levallois recurrent centripetal as being thinner. However, the interpretation of PC1 (which better captures elongation) proves not to be a good criterion for discriminating between strategies, with both methods showing a very wide range. Concerning the elongation of Levallois products, Boëda et al. (1990) also noticed the decrease of length/width ratio with each successive exploitation, resulting in short non-laminar flakes and core edge flakes. Mourre (2003) calls attention to the direction of the flake debitage axis being parallel to the plane of intersection of both surfaces in the case of Levallois core edge flakes. In the present study, the effect of this feature can be linked to a higher carenation index, which is captured by PC3. The visual exploration of the 3D meshes according to PC values did not seem to capture the relation between the debitage axis and the symmetry of blanks as an important feature of Levallois centripetal backed flakes (Meignen, 1996; Meignen, 1993). This is probably due to the inclusion of core edge flakes with a limited back in the experimental sample and its possible importance being overshadowed by other features better for discrimination captured by PC3 (IPA, carenation index and elongation index).

González-Molina et al. (2020) achieve an 80% accuracy when differentiating between discoidal and Levallois centripetal flakes. Although their study focuses on only exploitation phase flakes (with the presence of cortex having very little importance as a variable for differentiating methods), and dimensional variables have high importance, it shows the potential of using machine learning models for the identification of knapping methods. In contrast, the present study focuses on a concrete set of technological products independent of the exploitation phase, and the use of geometric morphometrics excludes dimensional variables. However, despite these differences, similar degrees of accuracy are obtained. Archer et al. (2021) also use geometric morphometrics and random forest to evaluate the differentiation between three strategies (Levallois, discoidal, and laminar). Although for the general performance of the models only accuracy is provided, their study does present a similar value to that of the present study. However, the classification of the two same classes as in the present study varies significantly, with an 87% accuracy for Levallois products and 40% in the differentiation of discoidal products. This contrasts heavily with the present study, where the classification is more balanced and the identification of backed products from the discoidal knapping strategy showed a slightly lower accuracy than the identification of products from the Levallois recurrent centripetal method (0.72 and 0.79, respectively).

Archer et al. (2021) also reported human analyst identification ratios on flakes for different archaeological sites with the "undiagnostic" class being the largest and usually above 60% (thus, only 35% of flakes were attributed to a knapping method). In both above-mentioned studies (Archer et al., 2021; González-Molina et al., 2020) and in the present study, the application of machine learning models notably increases the accuracy and predictions regarding the identification of knapping methods. However, extreme caution is strongly advisable when evaluating the findings since a controlled experimental assemblage does not mimic the complexity of the archaeological record.

The present study has employed multiple linear regression with common metrics of lithic analysis as predictors

to determine what features were captured by the PCs. The multiple linear regressions of both PC3 and PC1 presented moderate values of correlation, with more than 0.6 of the variance explained. However, this also implies that a good portion of the variance remains unexplained for both PCs. The remaining unexplained variance can be the result of several factors. Metric variables used as predictors were taken manually, and this results in some degree of error. Geometric morphometrics capture with higher resolution the same metric variables, thus resulting in a source of error when establishing correlations. Another source of the unexplained PC variance might come from additional metric features (and their interactions), which are recorded when exhaustive attribute analysis is undertaken for lithic analysis (such as the number, organization and flaking angle of previous removals). This suggests that the improvement of this research should take into account increasing sample size along with the incorporation of these analytical features.
Backed flakes detached from discoidal and Levallois recurrent centripetal methods have been the focus of this study. However, it is important to note that backed products are common to other flaking strategies such as Quina and SSDA (Bourguignon, 1996; Forestier, 1993) not included in the present study. Although in Western Europe the coexistence of Levallois and discoidal knapping methods with other knapping methods in the same archaeological levels is a subject of debate (Faivre et al., 2017; Grimaldi and Santaniello, 2014; Marciani et al., 2020; Ríos-Garaizar, 2017), the present model can be applied to assemblages where Levallois and Discoid knapping strategies coexist. For this, the study and evaluation of the operative chain and assemblage context and integrity are fundamental for the study of lithic technology (Soressi and Geneste, 2011). Thus, the operative chain and assemblage context should be considered prior to the application of geometric morphometrics and machine learning models for the identification of knapping methods.

5. Conclusions

Backed flakes are technological products that play special roles in the Discoid and Levallois recurrent centripetal methods (Boëda, 1993; Boëda et al., 1990; Slimak, 2003). These roles are the result of managing the lateral and distal convexities (Boëda et al., 1990), but also their systematic production can indicate their role as production objectives (Locht, 2003; Slimak, 2003). Additionally, the results from several sites show that they were commonly imported and exported (Geneste, 1988; Roebroeks et al., 1992; Turq et al., 2013), forming parts of toolkits. This frequent transport is possibly a result of their specific morpho-functional features (Delpiano et al., 2021), which resulted from their role in core management and debitage direction. Being detached from two technologically different knapping methods, it is expected that their morphological features differ and allow for the identification of the knapping method. With the use of geometric morphometrics, these morphological features can be quantified, and PCA for dimensionality reduction allows them to be employed in machine learning models.
PCA and machine learning models indeed capture the different morphological features derived from both knapping methods, resulting in an accuracy of 0.76 and an AUC of 0.8 in the case of the best model for differentiating between knapping strategies. Most of the importance for differentiating between the knapping methods was captured by only one variable (PC3), which multiple linear regressions showed to be correlated with the elongation index and mostly an interaction between IPA and the carenation index.
Geometric morphometrics in combination with dimensionality reduction methods (PCA) and machine learning models can offer high-resolution methods for the identification of knapping methods in lithic analysis although their application should not be independent from the study of the operative chain and assemblage technological context.
Acknowledgments
This research has been supported by the project SI1/PJI/2019-00488 funded by Comunidad Autónoma de Madrid and Universidad Autónoma de Madrid.

Author Contributions

FR and GBP conceived and designed the research and the experiments. GBP, BG, MB performed the experiments. GBP analyzed and curated the data. Original draft was written by GBP and FR. MB, FR, and BG reviewed and edited the manuscript. FR was responsible for funding acquisition. All the authors agreed on the final version of the paper.

References

Archer, W., Djakovic, I., Brenet, M., Bourguignon, L., Presnyakova, D., Schlager, S., Soressi, M., McPherron, S.P., 2021. Quantifying differences in hominin flaking technologies with 3D shape analysis. Journal of Human Evolution 150, 102912. https://doi.org/10.1016/j.jhevol.2020.102912

Archer, W., Pop, C.M., Rezek, Z., Schlager, S., Lin, S.C., Weiss, M., Dogandžić, T., Desta, D., McPherron, S.P., 2018. A geometric morphometric relationship predicts stone flake shape and size variability. Archaeological and Anthropological Sciences 10, 1991–2003. https://doi.org/10.1007/s12520-017-0517-2

Bergmeir, C., Benítez, J.M., 2012. Neural Networks in R using the Stuttgart Neural Network Simulator: RSNNS. Journal of Statistical Software 46. https://doi.org/10.18637/jss.v046.i07

Beyries, S., Boëda, E., 1983. Étude technoloogique et traces d'utilisation des éclats débordants de corbehem (pas-de-calais). Bulletin de la Société préhistorique française 80, 275–279. https://doi.org/https://doi.org/10.3406/bspf.1983.5455

Boëda, E., 1995a. Levallois: A volumetric construction, methods, a technique, in: Dibble, H.L., Bar-Yosef, O. (Eds.), The Definition and Interpretation of Levallois Technology, Monographs in World Archaeology. Prehistory Press, Madison, Wisconsin, pp. 41–68.

Boëda, E., 1995b. Caractéristiques techniques des chaînes opératoires lithiques des niveaux micoquiens de Külna (Tchécoslovaquie). Paléo 1, 57–72. https://doi.org/10.3406/pal.1995.1380

Boëda, E., 1994. Le concept levallois: Variabilité des méthodes, CNRS éditions. CNRS.

Boëda, E., 1993. Le débitage discoïde et le débitage levallois récurrent centripède. Bulletin de la Société Préhistorique Française 90, 392–404. https://doi.org/10.3406/bspf.1993.9669

Boëda, E., Geneste, J.-M., Meignen, L., 1990. Identification de chaînes opératoires lithiques du paléolithique ancien et moyen. Paléo 2, 43–80.

Bookstein, F.L., 1997b. Landmark methods for forms without landmarks: Morphometrics of group differences in outline shape. Medical Image Analysis 1, 225–243. https://doi.org/10.1016/S1361-8415(97)85012-8

Bookstein, F.L., 1997a. Morphometric tools for landmark data. Cambridge University Press.

Bordes, F., 1961. Typologie du paléolithique ancien et moyen, Publications de l'institut de préhistoire de l'université de bordeaux. CNRS Editions, Bordeaux.

Bordes, F., 1953. Notules de typologie paléolithique II : Pointes Levalloisiennes et pointes pseudo-levalloisiennes. bspf 50, 311–313. https://doi.org/10.3406/bspf.1953.3057

Bourguignon, L., 1996. La conception du debitage quina. Quaternaria Nova 6, 149–166.

Bradley, A.P., 1997. The use of the area under the ROC curve in the evaluation of machine learning algorithms. Pattern recognition 30, 1145–1159.

Breiman, L., 2001. Random forests. Machine Learning 45, 5–32. https://doi.org/10.1023/A:1010933404324

Brenet, M., 2013. Variabilité et signification des productions lithiques au paléolithique moyen ancien. L'exemple de trois gisements de plein-air du bergeracois (dordogne, france), BAR international series. Archaeopress, Oxford.

Brenet, M., 2012. Silex et roches métamorphiques au paléolithique moyen récent: Combemenue (corrèze) et chemin d'herbe (lot-et-garonne), in: Marchand, G., Querré, G. (Eds.), Roches Et Sociétés de La Préhistoire Entre Massifs Cristallins Et Bassins Sédimentaires : Le Nord-Ouest de La France Dans Son Contexte Européen. Presses universitaires de Rennes, pp. 379–393.

Brenet, M., Cretin, C., 2008. Le gisement paléolithique moyen et supérieur de combemenue (brignac-la-plaine, corrèze). Du microvestige au territoire, réflections sur les perspectives d'une approche multi-scalaire, in: Aubry, T., Almeida, F., Araújo, A.C., Tiffagom, M. (Eds.), Proceedings of the XV World Congress UISPP (Lisbon, 4-9 September 2006). Space and Time: Which Diachronies, Which Synchronies, Which Scales? / Typology Vs Technology, Sessions C64 and C65, BAR International Series. Archaeopress, Oxford, pp. 35–44.

Bustillo, M.A., Pérez-Jiménez, J.L., 2005. Características diferenciales y génesis de los niveles silíceos explotados en el yacimiento arqueológico de casa montero (vicálvaro, madrid). Geogaceta 38, 243–246.

Bustillo, M.Á., Pérez-Jiménez, J.L., Bustillo, M., 2012. Caracterización geoquímica de rocas sedimentarias formadas por silicificación como fuentes de suministro de utensilios líticos (mioceno, cuenca de madrid). Revista Mexicana de Ciencias Geológicas 29, 233–247.

Cortes, C., Vapnik, V., 1995. Support-vector networks. Machine learning 20, 273–297.

Courbin, P., Brenet, M., Michel, A., Gravina, B., 2020. Spatial analysis of the late middle palaeolithic open-air site of bout-des-vergnes (bergerac, dordogne) based on lithic technology and refitting. Journal of Archaeological Science: Reports 32, 102373. https://doi.org/https://doi.org/10.1016/j.jasrep.2020.102373

Cover, T., Hart, P., 1967. Nearest neighbor pattern classification. IEEE Trans. Inform. Theory 13, 21–27. https://doi.org/10.1109/TIT.1967.1053964

Cramer, J.S., 2004. The early origins of the logit model. Studies in History and Philosophy of Science Part C: Studies in History and Philosophy of Biological and Biomedical Sciences 35, 613–626. https://doi.org/10.1016/j.shpsc.2004.09.003

Delagnes, A., 1995. Variability within uniformity: Three levels of variability within the levallois system, in: Dibble, H.L., Bar-Yosef, O. (Eds.), The Definition and Interpretation of Levallois Technology, Monographs in World Archaeology. Prehistory Press, Madison, Wisconsin, pp. 201–211.

Delagnes, A., Meignen, L., 2006. Diversity of lithic production systems during the middle paleolithic in france. Are there any chronological trends?, in: Hovers, E., Kuhn, S.L. (Eds.), Transitions Before the Transition Evolution and Stability in the Middle Paleolithic and Middle Stone Age. Springer, pp. 85–107.

Delpiano, D., Gennai, J., Peresani, M., 2021. Techno-functional implication on the production of discoid and levallois backed implements. Lithic Technology 46, 171–191. https://doi.org/10.1080/01977261.2021.1886487

Duran, J.-P., 2005. L'industrie moustérienne des Ànecs (Rodès, Pyrénées-orientales, France). PYRENAE 36, 11–39.

Duran, J.-P., Soler, N., 2006. Variabilité des modalités de débitage et des productions lithiques dans les industries moustériennes de la grotte de l'arbreda, secteur alpha (serinyà, espagne). Bulletin de la Société Préhistorique Française 103, 241–262.

Faivre, J.-Ph., Gravina, B., Bourguignon, L., Discamps, E., Turq, A., 2017. Late middle palaeolithic lithic technocomplexes (MIS 5–3) in the northeastern aquitaine basin: Advances and challenges. Quaternary International 433, 116–131. https://doi.org/10.1016/j.quaint.2016.02.060

Fernandes, P., Morala, A., Schmidt, P., Séronie-Vivien, M.-R., Turq, A., 2012. Le silex du bergeracois: État de la question. Quaternaire Continental d'Aquitaine, excursion AFEQ, ASF 2012 2012, 22–33.

Fisher, R.A., 1936. The use of multiple measurements in taxonomic problems. Annals of Eugenics 7, 179–188.

Folgado, M., Brenet, M., 2010. Economie de débitage et organisation de l'espace technique sur le site du paléolithique moyen de plein-air de la mouline (dordogne, france), in: Conard, N., Delagnes, A. (Eds.), Settlement Dynamics of the Middle Paleolithic and Middle Stone Age. Kerns Verlag - (Tübingen Publications in Prehistory), Tübingen, pp. 427–454.

Forestier, H., 1993. Le Clactonien: mise en application d'une nouvelle méthode de débitage s'inscrivant dans la variabilité des systèmes de production lithique du Paléolithique ancien. pal 5, 53–82. https://doi.org/10.3406/pal.1993.1104

Frey, P.W., Slate, D.J., 1991. Letter recognition using holland-style adaptive classifiers. Machine learning 6, 161–182.

Friedman, J.H., 2002. Stochastic gradient boosting. Computational Statistics & Data Analysis 38, 367–378. https://doi.org/10.1016/S0167-9473(01)00065-2

Friedman, J.H., 2001. Greedy function approximation: A gradient boosting machine. Annals of statistics 29, 1189–1232.

Geneste, J.-M., 1988. Les industries de la grotte vaufrey: Technologie du debitage, economie et circulation de la matiere premiere lithique, in: Rigaud, J.-P. (Ed.), La Grotte Vaufrey à Cenac Et Saint-Julien (Dordogne) : Paléoenvironnements, Chronologie Et Activités Humaines, Mémoires de La Société Préhistorique Française (Revue). Société préhistorique française, Paris, pp. 441–517.

González-Molina, I., Jiménez-García, B., Maíllo-Fernández, J.-M., Baquedano, E., Domínguez-Rodrigo, M., 2020. Distinguishing discoid and centripetal levallois methods through machine learning. PLoS ONE 15, e0244288. https://doi.org/10.1371/journal.pone.0244288

Greenwell, B., Boehmke, B., Cunningham, J., Developers, G.B.M., Greenwell, M.B., 2019. Package 'gbm.' R package version 2.

Grimaldi, S., Santaniello, F., 2014. New insights into final mousterian lithic production in western italy. Quaternary International 350, 116–129. https://doi.org/10.1016/j.quaint.2014.03.057

Gunz, P., Mitteroecker, P., 2013. Semilandmarks: A method for quantifying curves and surfaces. Hystrix 24, 103–109. https://doi.org/10.4404/hystrix-24.1-6292
Gunz, P., Mitteroecker, P., Bookstein, F.L., 2005. Semilandmarks in three dimensions, in: Modern Morphometrics in Physical Anthropology. Springer, New York, pp. 73–98.
James, G., Witten, D., Hastie, T., Tibshirani, R., 2013. An introduction to statistical learning with applications in r, Second Edition. ed. Springer.
Karatzoglou, A., Meyer, D., Hornik, K., 2006. Support vector machines in r. Journal of Statistical Software 15, 1–28. https://doi.org/10.18637/jss.v015.i09
Karatzoglou, A., Smola, A., Hornik, K., Zeileis, A., 2004. Kernlab - an S4 package for kernel methods in r. Journal of Statistical Software 11, 1–20. https://doi.org/10.18637/jss.v011.i09
Kelly, H., 1954. Contribution à l'étude de la technique de la taille levalloisienne. Bulletin de la Société Préhistorique Française 51, 149–169. https://doi.org/10.3406/bspf.1954.3077
Kendall, D.G., 1984. Shape manifolds, procrustean metrics, and complex projective spaces. Bulletin of the London Mathematical Society 16, 81–121. https://doi.org/10.1112/blms/16.2.81
Kuhn, M., 2008. Building predictive models in r using the caret package. Journal of Statistical Software 28. https://doi.org/10.18637/jss.v028.i05
Kuhn, S.L., 2013. Roots of the middle paleolithic in eurasia. Current Anthropology 54, S255–S268. https://doi.org/10.1086/673529
Lantz, B., 2019. Machine learning with r: Expert techniques for predictive modeling. Packt publishing ltd.
Lenoir, M., Turq, A., 1995. Recurrent centripetal debitage (levallois and discoidal): Continuity or discontinuity?, in: Dibble, H.L., Bar-Yosef, O. (Eds.), The Definition and Interpretation of Levallois Technology, Monographs in World Archaeology. Prehistory Press, Madison, Wisconsin, pp. 249–256.
Locht, J.-L., 2003. L'industrie lithique du gisement de beauvais (oise, france): Objectifs et variabilité du débitage discoïde, in: Peresani, M. (Ed.), Discoid Lithic Technology: Advances and Implications, BAR International Series. Archaeopress, Oxford, pp. 193–209.
Marciani, G., Ronchitelli, A., Arrighi, S., Badino, F., Bortolini, E., Boscato, P., Boschin, F., Crezzini, J., Delpiano, D., Falcucci, A., Figus, C., Lugli, F., Oxilia, G., Romandini, M., Riel-Salvatore, J., Negrino, F., Peresani, M., Spinapolice, E.E., Moroni, A., Benazzi, S., 2020. Lithic techno-complexes in italy from 50 to 39 thousand years BP: An overview of lithic technological changes across the middle-upper palaeolithic boundary. Quaternary International 551, 123–149. https://doi.org/10.1016/j.quaint.2019.11.005
Martín-Viveros, J.I., Ollé, A., Chacón, M.G., Romagnoli, F., Gómez de Soler, B., Vaquero, M., Saladié, P., Vallverdú, J., Carbonell, E., 2020. Use-wear analysis of a specific mobile toolkit from the middle paleolithic site of abric romaní (barcelona, spain): A case study from level m. Archaeol Anthropol Sci 12, 16. https://doi.org/10.1007/s12520-019-00951-z
McPherron, S., 2019. E5 (beta version).
Meignen, L., 1996. Persistance des traditions techniques dans l'abri des canalettes (nant-aveyron). Quaternaria Nova 6, 449–64.
Meignen, L., 1993. Les industries lithiques de l'abri des Canalettes: cuche 2, in: Meignen, L. (Ed.), L'abri des Canalettes. Un habitat moustérien sur les grands Causses (Nant-Aveyron), Monographie du CRA. CNRS Ed., Paris, pp. 238–328.
Mitteroecker, P., Gunz, P., 2009. Advances in geometric morphometrics. Evolutionary Biology 36, 235–247. https://doi.org/10.1007/s11692-009-9055-x
Mourre, V., 2003. Discoïde ou pas discoïde? Réflexions sur la pertinence des critères techniques définissant le débitage discoïde, in: Peresani, M. (Ed.), Discoid Lithic Technology. Advances and Implications, BAR International Series. Archaeopress, Oxford, pp. 1–17.
O'Higgins, P., 2000. The study of morphological variation in the hominid fossil record: Biology, landmarks and geometry. Journal of Anatomy 197, 103–120. https://doi.org/10.1046/j.1469-7580.2000.19710103.x
Pasty, J.-F., Liegard, S., Alix, P., 2004. Étude de l'industrie lithique du site paléolithique moyen des Fendeux (Coulanges, Allier). bspf 101, 5–25. https://doi.org/10.3406/bspf.2004.12945
Pearson, K., 1901. On lines and planes of closest fit to systems of points in space. The London, Edinburgh, and Dublin Philosophical Magazine and Journal of Science 2, 559–572. https://doi.org/10.1080/14786440109462720
Quinlan, J.R., 2014. C4. 5: Programs for machine learning. Elsevier.
Quinlan, J.R., 1996. Improved use of continuous attributes in C4.5. jair 4, 77–90. https://doi.org/10.1613/

jair.279
Ridgeway, G., 2007. Generalized Boosted Models: A guide to the gbm package. R package vignette 2007.
Ríos-Garaizar, J., 2017. A new chronological and technological synthesis for late middle paleolithic of the eastern cantabrian region. Quaternary International 433, 50–63. https://doi.org/10.1016/j.quaint.2016.02.020
Roebroeks, W., Loecker, D.D., Hennekens, P., Leperen, M.V., 1992. "A veil of stones": On the interpretation of an early middle palaeolithic low density scatter at maastricht-belvédère (the netherlands). Analecta Praehistorica Leidensia 25| The end of our third decade: Papers written on the occasion of the 30th anniversary of the Institutte of prehistory, volume I 25, 1–16.
Romagnoli, F., Bargalló, A., Chacón, M.G., Gómez de Soler, B., Vaquero, M., 2016. Testing a hypothesis about the importance of the quality of raw material on technological changes at abric romaní (capellades, spain): Some considerations using a high-resolution techno-economic perspective. JLS 3, 635–659. https://doi.org/10.2218/jls.v3i2.1443
Rumelhart, D.E., Hinton, G.E., Williams, R.J., 1986. Learning representations by back-propagating errors. Nature 323, 533–536.
Schlager, S., 2017. Morpho and rvcg–shape analysis in r: R-packages for geometric morphometrics, shape analysis and surface manipulations, in: Statistical Shape and Deformation Analysis. Elsevier, pp. 217–256.
Simpson, E.H., 1951. The interpretation of interaction in contingency tables. Journal of the Royal Statistical Society: Series B (Methodological) 13, 238–241. https://doi.org/10.1111/j.2517-6161.1951.tb00088.x
Slimak, L., 2003. Les debitages discoïdes mousteriens: Evaluation d'un concept technologique, in: Peresani, M. (Ed.), Discoid Lithic Technology. Advances and Implications, BAR International Series. Archaeopress, Oxford, pp. 33–65.
Slimak, L., 1998. La variabilité des débitages discoïdes au paléolithique moyen: Diversité des méthodes et unité d'un concept. L'exemple des gisements de la baume néron (soyons, ardèche) et du champ grand (saint-maurice-sur-loire, loire). Préhistoire anthropologie méditerranéennes 7, 75–88.
Soressi, M., Geneste, J.-M., 2011. The history and efficacy of the chaîne opératoire approach to lithic analysis: Studying techniques to reveal past societies in an evolutionary perspective. PaleoAnthropology 2011, 334–350. https://doi.org/10.4207/PA.2011.ART63
Spackman, K.A., 1989. Signal detection theory: Valuable tools for evaluating inductive learning, in: Proceedings of the Sixth International Workshop on Machine Learning. Elsevier, pp. 160–163.
Team, R.C., 2019. R: A language and environment for statistical computing. R Foundation for Statistical Computing, Vienna, Austria.
Team, Rs., 2019. RStudio: Integrated development for r. RStudio, Inc., Boston, MA.
Turq, A., Roebroeks, W., Bourguignon, L., Faivre, G.-P., 2013. The fragmented character of middle palaeolithic stone tool technology. Journal of Human Evolution 65, 641–655. https://doi.org/10.1016/j.jhevol.2013.07.014
Walker, S.H., Duncan, D.B., 1967. Estimation of the probability of an event as a function of several independent variables. Biometrika 54, 167–179. https://doi.org/10.2307/2333860
Weihs, C., Ligges, U., Luebke, K., Raabe, N., 2005. klaR analyzing german business cycles, in: Data Analysis and Decision Support. Springer, pp. 335–343.
Wickham, H., Averick, M., Bryan, J., Chang, W., McGowan, L., François, R., Grolemund, G., Hayes, A., Henry, L., Hester, J., Kuhn, M., Pedersen, T., Miller, E., Bache, S., Müller, K., Ooms, J., Robinson, D., Seidel, D., Spinu, V., Takahashi, K., Vaughan, D., Wilke, C., Woo, K., Yutani, H., 2019. Welcome to the tidyverse. Journal of Open Source Software 4, 1686. https://doi.org/10.21105/joss.01686
Wright, M.N., Ziegler, A., 2017. Ranger: A fast implementation of random forests for high dimensional data in c++ and r. Journal of Statistical Software 77, 1–17. https://doi.org/10.18637/jss.v077.i01